Author Manuscript

Author Manuscript

Author Manuscript

Author Manuscript

HHS Public Access

Author manuscript

Cell. Author manuscript; available in PMC 2023 February 03.

Published in final edited form as:

Cell. 2022 February 03; 185(3): 513–529.e21. doi:10.1016/j.cell.2022.01.002.

Strain-level fitness in the gut microbiome is an emergent property of glycans and a single metabolite

Sun-Yang Park[1], **Chitong Rao**[1], **Katharine Z. Coyte**[1,7], **Gavin A. Kuziel**[1], **Yancong Zhang**[3,4], **Wentao Huang**[5,6], **Eric A. Franzosa**[3], **Jing-Ke Weng**[5,6], **Curtis Huttenhower**[3,4], **Seth Rakoff-Nahoum**[1,2,4,8,*]

[1]Division of Infectious Diseases and Division of Gastroenterology, Department of Pediatrics, Boston Children's Hospital, Boston, MA, USA

[2]Department of Microbiology, Harvard Medical School, Boston, MA, USA

[3]Department of Biostatistics, Harvard T.H. Chan School of Public Health, Boston, MA, USA

[4]Broad Institute of MIT and Harvard, Cambridge, MA, USA

[5]Whitehead Institute for Biomedical Research, Cambridge, MA, USA

[6]Department of Biology, Massachusetts Institute of Technology, Cambridge, MA, USA

[7]Present address: Division of Evolution & Genomic Sciences, School of Biological Sciences, University of Manchester, Manchester, UK

[8]Lead contact

SUMMARY

The human gut microbiota resides within a diverse chemical environment challenging our ability to understand the forces shaping this ecosystem. Here, we reveal that fitness of the Bacteroidales, the dominant order of bacteria in the human gut, is an emergent property of glycans and one specific metabolite, butyrate. Distinct sugars serve as strain-variable fitness switches activating context-dependent inhibitory functions of butyrate. Differential fitness effects of butyrate within the *Bacteroides* are mediated by species-level variation in Acyl-CoA thioesterase activity and nucleotide polymorphisms regulating an Acyl-CoA transferase. Using *in vivo* multi-omic profiles, we demonstrate *Bacteroides* fitness in the human gut is associated together, but not independently, with Acyl-CoA transferase expression and butyrate. Our data reveal that each strain of the *Bacteroides* exists within a unique fitness landscape based on the interaction of chemical

*Correspondence: seth.rakoff-nahoum@childrens.harvard.edu.

AUTHOR CONTRIBUTIONS

S-Y.P. and S.R.-N. designed the study, analyzed the data, and wrote the manuscript with input from the other authors. S-Y.P., C.R., G.A.K., W.H., and S.R.-N. performed the experiments. K.Z.C. performed digital imaging and analysis. Y.Z., E.A.F., and C.H. performed MGX, MTX, and MBX analysis. All authors contributed to the intellectual interpretation of results and the final contents of the manuscript.

DECLARATION OF INTERESTS

J.K.W. is a member of the SAB and a shareholder of DoubleRainbow Biosciences, Galixir, and Inari Agriculture. The other authors declare no competing interests.

SUPPLEMENTAL INFORMATION

Supplemental information can be found online at https://doi.org/10.1016/j.cell.2022.01.002.

components unpredictable by the effect of each part alone mediated by flexibility in the core genome.

Graphical Abstract

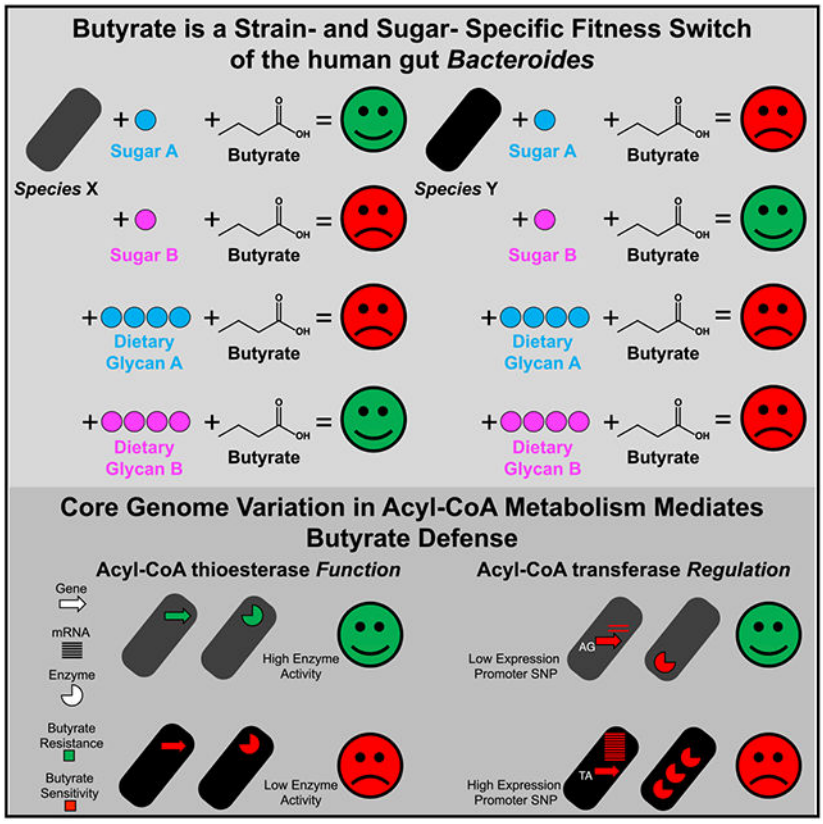

In brief

Each member of the human gut microbiome *Bacteroides* has a unique fitness landscape whereby depending on which glycan a strain uses, the metabolite butyrate is differentially inhibitory, and defense to butyrate is mediated by genetic variation among *Bacteroides* in Acyl-CoA metabolism.

INTRODUCTION

The gut microbiome is composed of an enormous magnitude and diversity of microorganisms residing in a chemically and molecularly complex ecosystem. Increasing evidence has highlighted the critical role of individual species' and strains' roles of the microbiome in human health, such as in protection from infection (Leshem et al., 2020; Pamer, 2016), immunity (Belkaid and Harrison, 2017; Honda and Littman, 2016; Macpherson et al., 2017), efficacy of vaccines (Hagan et al., 2019), immunotherapy (Zitvogel et al., 2018), drug metabolism (Koppel et al., 2017; Zimmermann et al., 2019), nutrition (Kolodziejczyk et al., 2019), and a multitude of human diseases (Barcik et al., 2020; Elinav et al., 2019; Plichta et al., 2019; Sherwin et al., 2019). Given the widespread impact of the microbiome on human health, there is an imperative to understand the forces

Author Manuscript Author Manuscript Author Manuscript Author Manuscript

Author Manuscript Author Manuscript Author Manuscript Author Manuscript

that shape the microbiome, in particular at the community and strain level (Ferreiro et al., 2018; Foster et al., 2017; Schmidt et al., 2018).

Carbohydrates are a major factor shaping the composition of the gut microbiome and mediate many of the effects of the microbiome on human health (Koropatkin et al., 2012; Porter and Martens, 2017; Sonnenburg and Bäckhed, 2016). Sugars such as dietary glycans are critical determinants of the fitness of the Bacteroidales, the predominant order of bacteria in the gut (Arumugam et al., 2011; Eckburg et al., 2005). The Bacteroidales are central to host health and disease, with specific Bacteroidales species and strains playing protective and pathogenic roles in human physiology and disease (Mazmanian et al., 2008; Wexler and Goodman, 2017). Survival of the Bacteroidales in the mammalian gut is dependent on the ability of each individual member to utilize and compete for the diverse array of glycans in the intestine (Patnode et al., 2019; Rakoff-Nahoum et al., 2014; Sonnenburg et al., 2010).

In addition to the wide range of carbohydrates, the gut ecosystem is rich in chemical and metabolic diversity (Donia and Fischbach, 2015; Integrative HMP (iHMP) Research Network Consortium, 2019). The chemical and metabolic composition of the gut, derived from components of diet as well as microbial and host metabolism, has important roles in human health (Sonnenburg and Bäckhed, 2016). One class of small molecules, the short-chain fatty acids (SCFAs), primary metabolites of host and microbial metabolism, is both abundant and dynamic across health and disease. SCFAs are critical to host activities from colonic epithelial metabolism and homeostasis, immunoregulation, cancer, and the gut-brain axis (Koh et al., 2016; Rooks and Garrett, 2016). The impact of the chemical and metabolite diversity of the intestinal ecosystem on the gut microbiome is largely unknown.

Here, we reveal that a microbial-derived small molecule, butyrate, is a context-dependent inhibitor of the human gut Bacteroidales. We find that fitness of Bacteroidales is a function of sugars and butyrate, whereby butyrate acts as a fitness-switch dependent on which specific sugar is utilized. Individual strains have idiosyncratic butyrate fitness switches across diverse sugars. The mechanism of species- and sugar-dependent inhibitory effects of butyrate is genetic variation in the function and regulation of Acyl-CoA metabolism within the *Bacteroides*. Our work demonstrates that strain-level fitness of the dominant order of bacteria in the human gut is an emergent property of specific dietary glycans and one microbial-derived small molecule butyrate, mediated by enzymatic and transcriptional regulatory variation in the core genome.

RESULTS

Butyrate displays strain-dependent inhibitory activity against the Bacteroidales

As abundant gut ecological commodities, we asked if the primary metabolite SCFAs affected the fitness of the Bacteroidales (Figure 1). We assayed a panel of SCFAs prevalent in the human gut (Koh et al., 2016) composed of a range of length (1–4 carbons), isomerization, and number of carboxylic acids groups (1 or 2) at physiological concentrations for effects on growth of a panel of 7 species of the Bacteroidales. Most SCFAs had either no or minimal effects on the Bacteroidales. However, the C4-monocarboxylated SCFA butyrate, exclusively produced by microbes (Lavelle and Sokol,

Author Manuscript Author Manuscript Author Manuscript Author Manuscript

2020), was found to be highly growth inhibitory to five of the seven Bacteroidales species tested (*B. eggerthi, Be*; *B. ovatus, Bo*; *B. uniformis, Bu*; *B. vulgatus, Bv*; *Parabacteroides merdae, Pm*), without notable effects on two (*B. fragilis, Bf*; *B. thetaiotaomicron, Bt*). Growth inhibition was specific to butyrate as compared to minimal fitness effects of the C3-monocarboxylated SCFA, propionate, or the C4-dicarboxylated SCFA, succinate.

We next examined the fitness effects of butyrate on an expanded collection of 53 human gut Bacteroidales isolates, encompassing multiple strains within a species (Figure 2A). Within the species *Bo* and *Bv*, for example, *Bo* CL03 and *Bv* CL09 strains were resistant to butyrate, while *Bo* ATCC 8483 and *Bv* ATCC 8482 strains were sensitive (Figure 2A). Together, these results identified the specific microbial metabolite butyrate as inhibitory to the Bacteroidales at the species and strain level.

Bacteroidales fitness is dependent on interactions of sugars and butyrate

The Bacteroidales use a diverse range of monosaccharides for energy to compete within the mammalian intestine (Koropatkin et al., 2012). We next assayed whether Bacteroidales susceptibility to butyrate was robust to a range of monosaccharides. These experiments yielded the striking finding that the inhibitory activity of butyrate was conditional on the monosaccharide utilized (Figure 2). For example, strains highly resistant to butyrate when grown in glucose (Glc) as the sole carbon source were rendered severely sensitive when utilizing *N*-Acetylgalactosamine (GalNAc) (Figures 2A and 2B). This inhibitory property was specific to butyrate, as growth in GalNAc did not render Bacteroidales strains sensitive to other SCFAs (Figure S1A). The differential inhibitory effects of butyrate across strains and sugars were not associated with growth rate (Figure S1B). Inhibition by butyrate was observed at concentrations as low as 2 mM (Figure S1C) within the physiological range of butyrate in the mammalian gut (Cummings et al., 1987; Koh et al., 2016). We reveal a hierarchy of strength of monosaccharides to tune fitness effects of butyrate: Glc, fructose (Fru) and mannose (Man) render most Bacteroidales resistant to butyrate, *N*-Acetylglucosamine (GlcNAc), galactose (Gal) and xylose (Xyl) mediate intermediate sensitivity, and rhamnose, ribose, and GalNAc render strains highly sensitive to butyrate (e.g., *Bt* VPI-5482) (Figures 2A and 2B). Importantly, we observed variation in the hierarchical strength of individual monosaccharides to tune butyrate-mediated *Bacteroides* fitness. For example, *B. fragilis* 9343 is highly resistant to butyrate in GlcNAc but highly sensitive in Xyl, whereas *B. ovatus* CL03 is substantially more resistant to butyrate in Xyl than in GlcNAc (Figures 2A and 2B). Together, these data reveal that butyrate interacts with individual monosaccharides on the fitness of the Bacteroidales. These interactions occur as a function of context, whereby the strength of distinct sugars differentially tunes butyrate-mediated fitness (sugar-strength), and as a function of intrinsic properties of the microbe in the same sugar, whereby specific strains are differentially resistant to butyrate (strain-strength).

While monosaccharides are the monomeric terminal products entering central metabolism, dietary oligomeric and polymeric glycans (which arrive undigested to the colon as microbiota-accessible carbohydrates; MACs) (Sonnenburg and Bäckhed, 2016) are critical forms of glycan utilized by the *Bacteroides* and are major drivers of *Bacteroides*

Author Manuscript Author Manuscript Author Manuscript Author Manuscript

composition (Patnode et al., 2019; Sonnenburg et al., 2010). Across a panel of 7 distinct dietary glycans there was a range of strain-level variation in susceptibility to butyrate (Figure S1D). Among *B. fragilis* species, utilizers of human milk oligosaccharides (HMOs) critical for colonizing the infant gut (Charbonneau et al., 2016; Marcobal et al., 2011), we observed a within-species, strain-level hierarchical strength of HMOs to tune butyrate-mediated fitness with strength increasing from 3-SL to LnNT to 2-FL (Figure 2C). As exemplified by *Bo* CL03, distinct plant- and animal-derived glycans can control the fitness effects of butyrate depending on which MAC is being utilized (Figure 2D). Cumulatively, these results demonstrate that depending on which MAC among the glycan diversity of the human diet composed of milk, plant, and animal glycans a given *Bacteroides* strain utilizes, there is a dynamic strain-specific range of fitness effects of butyrate.

Unpredictable interactions of glycan components with butyrate on strain-level fitness

Comparing the fitness effects of *Bacteroides* strains for monosaccharides and MACs revealed a striking discordance of the inhibitory effects of butyrate for specific polymers and the monomers of which the glycan is composed (cognate polymer-monomer pairs). For some MACs, there was concordance between cognate polymer-monomer pairs, such as *Bacteroides* members resistant to butyrate in the glucan pullulan and the fructan levan, which also demonstrated resistance to butyrate in Glc or Fru monomers (Figures 2A, 2B, 2D, and S1B). However, for certain polymers, we observed phenotypic discordance in the effects of butyrate for polymer-monomer pairs. For example, *Bo* CL03 was highly resistant to butyrate in the monomers arabinose, Gal, Glc, and Man but highly sensitive to butyrate in cognate heteropolymers, arabinogalactan, orglucomannan (Figures 2A, 2B, and 2D). Sensitivity to butyrate in these polymers was not a property of the individual monomers of these heteropolymers in combination (Figure S1E).

We next analyzed the inhibitory function of butyrate for *Bacteroides* species in cognate pairs of monomer and homo- and hetero-dimers. *Bo* CL03, resistant to butyrate in Glc and Fru, was also resistant in the Glc homodimer maltose (α1,4) and the Glc-Fru heterodimer sucrose (α1,β2) (Figure 2E). However, this strain was highly sensitive to butyrate in the Glc homodimers cellobiose (β1,4) and the Glc-Fru heterodimer palatinose (α1,6) (Figure 2E). Furthermore, we find species-level variation in discordance of butyrate-mediated fitness between monomers and dimers. *B. xylanisolvens* (*Bx*) CL03 was resistant to butyrate in Glc but sensitive in all Glc homodimers including cellobiose (Figure 2E). In contrast, *Bu* CL03 was resistant to butyrate in maltose and cellobiose (Figure 2E). Together, these results demonstrate species-level properties of glycan components independent of their overall combination in mediating the fitness effects of butyrate on the *Bacteroides*.

Butyrate affects microbiome community composition in a glycan-dependent manner

The composition of *Bacteroides* communities is driven by competition based on utilization of dietary glycans (Patnode et al., 2019; Sonnenburg et al., 2010). Our findings suggested that the composition of *Bacteroides* communities could be a property of species- and glycan-specific fitness as a function of both the specific glycan and butyrate. To determine if butyrate impacts the relative abundance of *Bacteroides* species *in vivo*, we colonized germ-free mice that were fed diets with either one or both of two prebiotic and health-relevant

Author Manuscript Author Manuscript Author Manuscript Author Manuscript

MACs, inulin and pectin (Koh et al., 2016), as the sole dietary glycan with a community of four *Bacteroides* species demonstrating distinct fitness effects of butyrate as a function of inulin and pectin *in vitro* (Figure 2F). Administration of butyrate led to significant impact on the fitness of each of the four species of *Bacteroides* in mice fed both dietary glycans (Figure 2G). With the exception of *Bc*, the fitness effects of butyrate on each *Bacteroides* species were glycan specific, with significant differences of the impact of butyrate on each *Bacteroides* species fitness depending on the specific dietary glycan (Figure 2G) correlating with the glycan-specific fitness effects of butyrate on each species *in vitro*. Together, these experiments demonstrate both that butyrate can impact the relative fitness of *Bacteroides in vivo* and impact species-level fitness in a glycan-dependent manner.

Butyrate induces sugar- and species-dependent stress responses

We next sought to determine the mechanistic basis of the interaction between butyrate and sugars on *Bacteroides* species-level fitness. To begin, we investigated the global transcriptional responses via RNA sequencing (RNA-seq) of the butyrate-resistant *B. thetaiotaomicron* VPI 5482 (herein *Bt*) and the butyrate-sensitive *B. vulgatus* ATCC 8482 (herein *Bv*) in Glc after a short pulse with different SCFAs (Table S2). Few genes were specifically regulated by butyrate in either strain, with the notable exception of upregulation in *Bt* of genes involved in biosynthesis of branched-chain amino acids (BCAAs) (*ilv* and *leu* operons) (Figures 3A and S2A). In both species, all SCFAs downregulated NADH-dehydrogenase genes (Figure 3A), which have been shown to be upregulated in response to intracellular acidification in bacteria (Kannan et al., 2008), suggesting that species-specific resistance was not a result of differential intracellular acidification by butyrate. Exposure to SCFAs did not result in intracellular acidification in the butyrate-sensitive *Bv*, nor did we observe differences in intracellular pH between inhibitory (butyrate) or non-inhibitory SCFAs (acetate or succinate) (Figure S2B). To determine the transcriptional response to butyrate as a function of sugar strength, we compared transcriptional responses of *Bv* to butyrate when grown in Glc, GlcNAc, Gal, or Xyl, which have increasing tuning of butyrate sensitivity (Table S2). Across sugars there was greater induction of stress-response genes such as Hsp family members and GroES with increasing sugar strength (Figure 3B). This suggests that butyrate caused a different degree of cellular stress depending on which sugar was being utilized. Indeed, we found differential cell membrane damage by butyrate dependent on sugar, with minimal membrane damage and bacteriostatic effect of butyrate in Glc in *Bv*, but not *Bt* other SCFAs, and severe membrane damage and subsequent cell death after treatment with butyrate in Gal (Figures 3C, 3D, and S2C). Together, these results demonstrate that butyrate induces species-specific cellular stress responses, membrane damage, and cell death in the *Bacteroides* and that the strength of cellular stress and bacteriostatic versus bactericidal function is sugar dependent.

An Acyl-Coenzyme A metabolic defense system in the *Bacteroides*

To dissect the mechanism by which butyrate is differentially inhibitory to the *Bacteroides*, we constructed a genome-wide transposon (Tn) mutagenesis library of *Bt* to identify the genetic determinants of butyrate resistance in *Bt* which demonstrates high level resistance to butyrate. Tn insertion in the BT_3942 gene conferred the greatest fitness disadvantage in butyrate among 14 genes with significant loss of fitness (Figure 4A). BT_3942 is an Acyl-

Author Manuscript Author Manuscript Author Manuscript Author Manuscript

coenzyme A (Acyl-CoA) thioesterase, predicted to hydrolyze Acyl-CoAs into free fatty acyl groups and coenzyme A (CoA) (Figure 4B). Targeted non-polar deletion of BT_3942 demonstrated sensitivity to butyrate at concentrations as low as 2 mM (Figure S3A) and in complex media with variable sugar concentration (Figure S3B). Complementation of *Bt* Δ3942 confirmed that this Acyl-CoA thioesterase gene confers resistance to butyrate (Figure 4C). Resistance was specific to butyrate as *Bt* Δ3942 did not become sensitive to other SCFAs (Figure S3C). Together, these data demonstrate that resistance to butyrate in *Bt* is mediated by an Acyl-CoA thioesterase.

To identify the genetic determinants that confer butyrate sensitivity in *Bv*, which demonstrates high sensitivity to butyrate, we performed transposon sequencing (Tn-seq) in *Bv* (Table S3). Tn insertion in the genes BVU_1163 and BVU_1164, which compose an operon, generated the greatest gain of resistance to butyrate among 91 genes with significant gain of resistance phenotype (Figures 4D and 4E). BVU_1163 is annotated as a putative Acyl-CoA transferase predicted to reversibly transfer CoAs from Acyl-CoAs to acetate (Figure 4E). Enzymatic assays with recombinant protein BVU_1163 revealed transferase activity for propionyl, butyryl, and succinyl-CoA substrates, but not the medium-chain hexanoyl-CoA (Figure S3D). Deletion of BVU_1163 (*Bv* Δ1163) rendered *Bv* partially resistant to butyrate in Glc, which was phenotypically complemented by expression of BVU_1163 (Figure 4F). These findings demonstrate that sensitivity to butyrate in *Bv* is mediated by an Acyl-CoA transferase. Expression of Acyl-CoA thioesterase BT_3942 conferred resistance to the naturally sensitive *Bv*, while expression of the Acyl-CoA transferase BVU_1163 conferred sensitivity in the naturally resistant *Bt*, demonstrating a common, opposing pathway of Acyl-CoA metabolism susceptibility in these two strains (Figure 4F). Together, our data demonstrate that Acyl-CoA metabolism acts in metabolic defense to the inhibitory effects of butyrate in the *Bacteroides*.

Butyrate uptake and metabolism by the *Bacteroides*

To determine if extracellular butyrate is taken up and converted metabolically by the *Bacteroides*, we pulsed naturally resistant *Bt* and naturally sensitive *Bv* with ^{13}C butyrate and measured ^{13}C labeling of intracellular Acyl-CoA metabolites in bacterial lysates after 30 min. ^{13}C labels were present in the forms of butyryl-CoA and to a lesser extent, acetyl-CoA, but not propionyl CoA in both *Bt* and *Bv* with notably a greater extent of ^{13}C-incorporation into butyryl-CoA in *Bv* (Figures 4G and S3E).

We next measured Acyl-CoA and free CoA pools after butyrate pulse yet before growth inhibition (Figure S3F) in *Bt* wild type (WT) and the butyrate-sensitive isogenic mutant *Bt* Δ3942 as well as in *Bv* WT and the partially butyrate-resistant isogenic mutant *Bv* Δ1163. In *Bt* WT, there was no significant change after butyrate pulse in acetyl-CoA, propionyl-CoA, or free CoA but moderate yet significant accumulation of butyryl-CoA (2-fold) (Figures 4H and S3G). In *Bv* WT, butyrate pulse led to a greater increase in butyryl-CoA levels compared to *Bt* and depletion of acetyl-CoA, propionyl CoA, and free CoA (Figures 4H and S3E). There was significant accumulation of butyryl-CoA in the butyrate-sensitive *Bt* Δ*3942* compared to *Bt* WT and depletion of acetyl-CoA and CoA, but not of propionyl-CoA (Figures 4H and S3G). Accumulation of butyryl-CoA as a result of BT_3942 deletion

Author Manuscript Author Manuscript Author Manuscript Author Manuscript

was confirmed by ^{13}C butyrate tracing (Figure 4G). Propionyl-CoA levels were unchanged between *Bv* WT and *Bv Δ1163* (Figure 4H). *Bv* Δ1163, despite being partially sensitive to butyrate, had higher levels of acetyl-CoA after butyrate pulse then that of healthy *Bv* WT in the absence of butyrate (Figure 4H). *Bv* Δ1163 demonstrated significantly less accumulation of butyryl-CoA after butyrate pulse compared to *Bv* WT (Figures 4H and S3G). Decreased accumulation of butyryl-CoA as a result of BVU_1163 deletion was confirmed by ^{13}C butyrate tracing (Figure 4G). Together, these data demonstrate that extracellular butyrate is taken up by *Bacteroides* and metabolized predominantly into butyryl-CoA, differentially impacts Acyl-CoA pools among *Bacteroides* species and as a function of Acyl-CoA thioesterase and Acyl-CoA transferase activity, and that butyryl-CoA accumulation correlates with the toxic effects of butyrate.

Sugar tuning of butyrate-mediated fitness via synergy in Acyl-CoA metabolism

In the absence of the Acyl-CoA transferase, *Bv* Δ1163 is partially resistant to butyrate in Glc but remains sensitive in Gal (Figure S4A), suggesting the existence of mechanisms in addition to the Acyl-CoA transferase BVU_1163 that mediate sugar-specific sensitivity to butyrate. To gain insight into the mechanism by which different sugars tune *Bacteroides* fitness to butyrate, we performed a synthetic fitness Tn-seq in *Bv* Δ1163 in Gal (Table S3). Four of the top five genes in which insertions leading to the greatest gain of fitness to butyrate in Gal occurred in two operons, BVU_2720/2719 and BVU_0575/0574 (Figure 5A). Remarkably, both BVU_0574 and BVU_2719 are predicted Acyl-CoA synthetases (Figure 5B). Notably, BVU_2719 (and the *Bt* homolog, BT_2782) was induced to a greater extent in Gal compared to Glc in both *Bv* and *Bt* and is repressed by butyrate in *Bv* in Gal (Figure S4B). Deletion of the BVU_0574 or BVU_2719 resulted in full resistance to butyrate in Glc and Gal in the *Bv* Δ1163 background but not in *Bv* WT background (Figure 5C). The Acyl-CoA synthetases did not have the same synergistic strength, as *Bv* Δ1163 Δ2719 showed greater resistance to butyrate in Gal compared with *Bv* Δ1163 Δ0574 (Figure 5C). Importantly, butyrate pulse in the *Bv* Δ1163 Δ0574 strain did not result in accumulation of butyryl-CoA, consistent with full resistance to butyrate (Figure S4C).

To address genetic mechanisms mediating the fitness effects of butyrate at the strain-level, we performed Tn-seq in *Bv* CL09 which is resistant to butyrate in Glc but sensitive in Gal and Xyl (Figures 2A and 2B) after selection in Gal in the presence of butyrate (Table S3; Figure S4D). This revealed gain-of-resistance insertions in AGXZ_01713 (Acyl-CoA transferase BVU_1163) and AGXZ_02243 and AGXZ_00341 (each of the Acyl-CoA synthetases, BVU_0574 and BVU_2719), each of which is 100% identical by amino acid (AA) between *Bv* ATCC and *Bv* CL09 (Table S3; Figure S4D). In *Bv* CL09, deletion of BVU_1163 or BVU_2719 conferred resistance to butyrate in Gal but not Xyl (Figure S4E). Deletion of both BVU_1163 and BVU_2719 resulted in resistance to butyrate in Xyl (Figure S4E). Together, these data demonstrate that synergy in Acyl-CoA metabolic genes mediates the hierarchical strength of sugars on fitness effects of butyrate in the *Bacteroides* at the species and strain level.

Author Manuscript Author Manuscript Author Manuscript Author Manuscript

Coenzyme A metabolic defense is tuned by a hierarchy of branched-chain AAs

Tn-seq in butyrate-resistant *Bt* revealed that 7 of the 14 genes with significant loss of resistance to butyrate belonged to the *ilv* (4 of 5 genes) and *leu* (3 of 5 genes) operon (Figures 4A and S4F), many of which were upregulated in Glc compared to Gal (Table S4). We reasoned that the BCAAs, end products of biosynthesis mediated by *ilv* and *leu* operons, might control resistance to butyrate in *Bt*. Remarkably, isoleucine (Ile), but not leucine (Leu) or valine (Val), conferred resistance to butyrate in *Bt* Δ3942 and *Bv* in Glc (Figure 5D) but not in Gal (Figure 5E). However, in *Bv* Δ1163, Ile conferred resistance to butyrate in Gal (Figure 5E). In *Bv* Δ1163 Δ0574, but not *Bv* Δ1163, Leu conferred resistance to butyrate in Gal (Figure 5E). Unexpectedly, in *Bv* Δ1163 Δ2719, which is resistant to butyrate in Glc and Gal, we observed that the addition of Val resulted in reversal of resistance, rendering this mutant sensitive to butyrate via a pathway counteracted by Ile (Figure 5E). We found examples of sugar-specific BCAA tuning in natural strains (Figure 5F) analogous to each *Bv* mutant of Acyl-CoA metabolism (Figure 5E). For example, Ile, but not Leu, conferred resistance in Gal in *Be* DSM (analogous to *Bv* Δ1163 in Gal), while Leu, but not Val, was able to confer resistance to butyrate in Glc (analogous to *Bv* Δ1163 Δ0574 in Gal). Addition of Val resulted in reversal of resistance in *B. dorei* 9-1-6 (analogous to *Bv* Δ1163 Δ2719) but not in *Bx* 1-1-30 (Figure 5F). These results suggest that *Bacteroides* species have a spectrum of Acyl-CoA metabolic states tunable by specific sugars and distinct BCAAs.

Species-level variation in Acyl-CoA thioesterase function among the *Bacteroides*

We next sought to determine the mechanism of species-level variation of the fitness effects of butyrate among the *Bacteroides*. Comparison of AA sequences revealed that the predicted Acyl-CoA thioesterase BT_3942 was poorly conserved among the *Bacteroides* (Figure S5A), sharing only 51% AA identity with a homolog BVU_0767 from butyrate-sensitive *Bv* (Figures 6A and S5B). Expression of BT_3942, but not BVU_0767, conferred resistance to both *Bt* Δ3942 and *Bv* WT (Figure 6B). Recombinant protein BT_3942 and BVU_0767 demonstrated different substrate specificity for hydrolysis of short chain lengths of Acyl-CoAs and propionyl- and butyryl-CoA but not medium or long chain Acyl-CoAs, with BT_3942 demonstrating substrate preference for butyryl-CoA (Figures 6C and S5C). Together, these results demonstrate that within *Bacteroides*, differences in the gene function of an Acyl-CoA thioesterase can mediate the variable fitness effects of butyrate.

Promoter polymorphisms mediate species-level variation in inhibitory effects of butyrate

As opposed to poor conservation of the Acyl-CoA thioesterase between *Bt* and *Bv*, the Acyl-CoA transferase BVU_1163 was highly conserved among the *Bacteroides* (Figure S5D), showing 83% AA identity with BT_3193 (Figures 6D and S5E). BT_3193 rendered both *Bv* Δ1163 and *Bt* sensitive to butyrate, comparable to that of BVU_1163 (Figure 6E). This suggests that the difference in butyrate sensitivity of *Bt* and *Bv* may be due to differential regulation of BT_3193 versus BVU_1163. Remarkably, BT_3193 was downregulated in *Bt*, while BVU_1163 was upregulated in *Bv* (Figure 6F) with corresponding differences in protein levels between these two species (Figure S5F). At the strain level, similar to the species level, there was greater expression of BVU_1163 in *Bv* ATCC (sensitive to butyrate in Glc) compared to *Bv* CL09 (resistant to butyrate in Glc) (Figure S5G). Thus, we observe

Author Manuscript Author Manuscript Author Manuscript Author Manuscript

an association between gene expression of this conserved Acyl-CoA metabolic gene and species- and strain-level variation in the fitness effect of butyrate.

To determine if differential expression of the Acyl-CoA transferase genes in *Bt* versus *Bv* is due to intrinsic properties of a specific promoter among *Bacteroides*, we cloned the promoter regions of BT_3193 (p*Bt*) and BVU_1163 (p*Bv*) upstream of either the BT_3193 or BVU_1163 operon, respectively, generating a panel of species-specific promoter-gene hybrid constructs (Figures 6G). The *Bv* promoter drove significantly greater expression of either gene compared to the *Bt* promoter, suggesting that differential gene regulation is due to species-specific intrinsic promoter strength (Figure 6G, left). To determine if high or low gene expression driven by the *Bv* or *Bt* specific promoters was sufficient to confer sensitivity to butyrate, the engineered strains harboring plasmids expressing each of the six hybrid pairs (no promoter, p*Bv*, or p*Bt* with BT_3193 or BVU_1163) were grown with or without butyrate. Remarkably, the strong, high-expression *Bv* promoter, but not the weak, low-expression *Bt* promoter (Figure 6G, middle), was sufficient to confer butyrate sensitivity to *Bv* Δ1163 (Figure 6G, right) and across a panel of naturally resistant *Bacteroides* species (Figure S5F) and strains (Figure S5I). Controlled inducible expression of BVU_1163 induced dose-dependent sensitivity in *Bv* as a function of sugar strength and *Bv* Δ1163 and *Bv* Δ1163 Δ0574 background (Figure S5J). Together, these data demonstrate that species-specific expression of a conserved Acyl-CoA transferase gene is regulated by species-specific promoter region to confer *Bacteroides* differential sensitivity to butyrate.

Species-level variation in butyrate sensitivity was encoded within 200 base pairs of the strain-specific promoter region of the Acyl-CoA transferase BVU_1163/BT_3193 (Figure 6G). Transcription initiation occurs by binding of the bacterial RNA polymerase holoenzyme complex to specific sequences of the promoter. Comparison of the *Bacteroides* −7 and −33 regions (Bayley et al., 2000; Lim et al., 2017; Mimee et al., 2016) revealed conservation of −7 region sequence TANNTTTG (Figure 6H). We observed a double nucleotide polymorphism (TTAG for p*Bt* and TTTA for p*Bv*) and a four-nucleotide difference in location of the −33 region between the *Bt* and *Bv* Acyl-CoA transferase promoters (Figure 6H). To determine the role of these species-specific promoter sequence variations in regulation of Acyl-CoA transferase gene expression, we made a series of constructs in −33 region nucleotide and location polymorphisms on the *Bv* high expression endogenous promoter backbone and the *Bt* low expression endogenous promoter backbone (Figure 6I, left). Remarkably, replacement of the *Bv* −33 region with the *Bt* −33 region nucleotide polymorphism (TTTA to TTAG) at its own or the *Bt* −33 region location (four-nucleotide spacer deletion) converted the *Bv* promoter into a low-expression promoter (Figure 6I, middle) and conferred resistance to butyrate (Figure 6I, right). Conversely, replacement of the *Bt* −33 region with the *Bv* −33 region nucleotide polymorphism (TTAG to TTTA) at its own or the *Bv* −33 region location (4 nucleotide spacer addition) converted the *Bt* promoter into a high-expression promoter (Figure 6I, middle) and conferred sensitivity to butyrate (Figure 6I, right). Together these results demonstrate that species-specific nucleotide and location polymorphisms encoded in *cis* at the −33 promoter region of a conserved Acyl-CoA transferase gene mediate variation in sensitivity of the *Bacteroides* to butyrate.

Author Manuscript Author Manuscript Author Manuscript Author Manuscript

Lower expression of BVU_1163 in *Bv* CL09, compared to *Bv* ATCC, correlated with strain-level differences in sensitivity to butyrate (Figure S5G). However, the promoter sequences of BVU_1163 are 100% identical within species between *Bv* ATCC and *Bv* CL09 (Figure S5K), suggesting that while −33 promoter *cis*-acting factors are responsible for regulation of Acyl-CoA transferase, c/s-independent factors may be responsible for differential mRNA levels of Acyl-CoA transferase at the strain level. To identify candidate strain-specific regulators of Acyl-CoA transferase expression, we performed RNA-seq in *Bv* CL09 after pulse of butyrate in Glc (Table S2) and compared global transcriptional responses to butyrate between *Bv* CL09 and *Bv* ATCC. We identified 87 genes demonstrating strain-specific regulation in response to butyrate (Table S2; Figure S5L). Of these, 74 were induced by butyrate specifically in *Bv* CL09, including 7 transcriptional regulators, two of which were anti-sigma factors AGXZ_01245 and AGXZ_00606 (Table S2) serving as candidates of *trans*-acting factors mediating *cis*-independent regulation of Acyl-CoA transferase gene expression at the strain level.

Acyl-CoA transferase expression and butyrate levels correlate with *Bacteroides* fitness *in vivo*

Our *in vitro* approach revealed that *Bacteroides* fitness is conditional on both butyrate and the expression level of the Acyl-CoA transferase, BT_3193/BVU_1163, whereby butyrate is inhibitory if the *Bacteroides* member expresses high levels of BT_3193/BVU_1163 (Figure 7A). We next sought evidence of whether *Bacteroides* fitness in the human gut is a function of butyrate and expression level of this conserved Acyl-CoA transferase. This required a multi-omics *in vivo* dataset simultaneously capturing metagenomes (MGX; BT_3193/BVU_1163 DNA abundance as a proxy for *Bacteroides* fitness), metatranscriptomes (MTX; relative expression of BT_3193/BVU_1163 RNA), and metabolomes (MBX; concentration of SCFAs, including butyrate), all from the same human fecal sample. Using the Inflammatory Bowel Disease Multi'omics Database (Lloyd-Price et al., 2019), we selected 88 longitudinal samples from 26 healthy subjects with matched MGX, MTX, and MBX data. We tested for associations between *Bacteroides* abundance and expression level of BT_3193/BVU_1163 under different gut metabolite levels. This analysis, independent of choice of metabolomics normalization method, revealed a significant negative correlation between *Bacteroides* abundance and the relative expression of BT_3193/BVU_1163 in high butyrate, and no correlation in either low butyrate or high succinate (Figures 7B and S6A) or between butyrate and BCAA (Figure S6B). Together, these data suggest that *Bacteroides* fitness *in vivo* is a function of both butyrate and expression of a conserved Acyl-CoA transferase in the human gut.

DISCUSSION

For the *Bacteroides*, the predominant Gram-negative bacteria of the human intestine, survival in the gut is dependent on the ability of each strain to utilize dietary and host sugars. We have revealed a context-dependent inhibitory function of the specific metabolite butyrate where one microbe-derived small molecule acts as a fitness switch depending on the specific sugar utilized and in which individual strains have distinct switches across sugars (Figure 7C, left). Our work demonstrates strain-level fitness of members of the

Author Manuscript Author Manuscript Author Manuscript Author Manuscript

gut microbiome as an emergent property (West-Eberhard, 2019) based on the interaction of components across molecular class unpredictable by the effect of each part alone. Furthermore, our findings uncover that each strain of the *Bacteroides* has a unique norm of reaction (Woltereck, 1909) for each sugar it can utilize. The mechanism of these non-linear reaction norms is within *Bacteroides* genetic variation in Coenzyme A metabolism which integrates these environmental chemical factors into dynamic fitness phenotypes. Elucidation of the emergent properties of the fitness of members of the gut is instrumental to our understanding of the context-dependent rules that govern the structure of the gut microbiome, its hierarchical organization, and attempts to engineer this ecosystem in health and disease.

Our study reveals a role of the specific SCFA butyrate in gut microbiota ecology. SCFAs play important roles in mammalian health. In microbe-microbe interactions in the gut, these primary metabolites have long been appreciated to be important in positive fitness interactions in microbial ecosystems based on syntrophy, in which bacteria utilize these substrates as energy sources via assimilation or as electron acceptors (Fischbach and Sonnenburg, 2011). Recent work has shown that SCFAs can inhibit Enterobacteriaciae, such as *Klebsiella pneumonia* and *Salmonella enterica*, through acidification of the intracellular compartment (Jacobson et al., 2018; Sorbara et al., 2019). Of the SCFAs, butyrate is distinctive in a numbers of ways: (1) it is uniquely made by specific bacteria, notably the Lachnospiraceae (as opposed to other SCFAs that may be made by a wide range of microbes and also the host) (Lavelle and Sokol, 2020), (2) with rare exceptions (Ziels et al., 2019), it is not used as an energy source by bacteria, and (3) it plays unique roles in host biology and fitness from roles in gut epithelial homeostasis and immunoregulation as an energy source, signaling molecule, and epigenetic modifier (Koh et al., 2016). Thus, it is tempting to speculate that the emergent properties of distinct sugars and butyrate reflects eco-evolutionary interactions playing out between butyrate-producing organisms and individual *Bacteroides* strains across glycan niches balanced over evolutionary time by host fitness.

We found that butyrate, but not other SCFAs, caused rapid cellular stress, membrane damage, and cell death, conditional on which sugar is being utilized and varying among the *Bacteroides*. Species- and sugar-dependent inhibitory function of butyrate is due to variation within the *Bacteroides* in both the function and regulation of Acyl-Coenzyme A metabolism. By identifying a specific inhibitory function of butyrate and elucidating a species-specific and sugar-dependent Coenzyme A-based metabolic defense system, our work presents a connection between growth inhibition and metabolism distinct from known links with growth rate, nutrient limitation, the stringent response, and oxidative stress (Stokes et al., 2019). It will be of interest to determine whether these Acyl-CoA metabolic enzymes evolved primarily in defense to butyrate or as a secondary function and whether the role of these enzymes is a general feature of bacteria across environments or specific to the metabolic versatility of *Bacteroides* and the gut ecosystem.

Our work suggests that several non-mutually exclusive mechanisms may mediate species- and sugar-level variation in the *Bacteroides* butyrate fitness switch. We discovered that the mechanism governing resistance to butyrate was variation in short Acyl-CoA thioesterase

Author Manuscript Author Manuscript Author Manuscript Author Manuscript

and transferase activity among the *Bacteroides*. ^{13}C tracing experiments and metabolite analysis suggest the conversion and accumulation of butyryl-CoA as a mechanism mediating the toxic effects of butyrate on the *Bacteroides* (Figure 7C, right) as an antimetabolite and/or metabolic poison. We found that specific BCAAs tuned the strain- and sugar-dependent toxicity of butyrate. This may occur through modulating specific Acyl-CoA and/or free acyl intracellular metabolites, such as acetyl-CoA, by Ile and Leu or propionyl-CoA by Val via BCAA catabolism by the BCKDH enzyme complex. Alternatively, our demonstration of a mechanistic role of a putative medium/long chain Acyl-CoA synthetase suggests that the protective (Ile, Leu) and detrimental (Val) role of specific BCAAs may be due to their role as precursors in the synthesis of functionally distinct and strain- and sugar-variable odd- (Ile, Leu) or even- (Val) length outer-membrane branched lipids (Kaiser and Heinrichs, 2018). We found phenotypic discordance between monomeric, dimeric, and polymeric sugars, suggesting that sensing of specific sugars, such as through two components systems (Schwalm et al., 2017), may play a regulatory role in modulating the effects of butyrate in the *Bacteroides*.

We found that variation in the enzymatic function of an Acyl-CoA thioesterase and regulation of an Acyl-CoA transferase by nucleotide polymorphisms in the RNA polymerase binding site at the −33 promoter region mediated differential resistance to butyrate among the *Bacteroides*. Strain-level variation in accessory genomes (Greenblum et al., 2015; Pasolli et al., 2019; Sberro et al., 2019; Zeevi et al., 2019) is well appreciated in adaptive functions in microbe-microbe, environmental, and host interactions both among the *Bacteroides* and in the gut microbiota at large, such as by encoding type-VI secretion systems, biosynthetic gene clusters, and polysaccharide utilization. By demonstrating a role for variation in Acyl-CoA metabolic genes, our work suggests that in addition to the accessory genome, the core genome may be under selection in members of the gut microbiota with strain-specific trade-offs between the role of central metabolism in bacterial physiology and ecological roles in diet- and microbe-microbe metabolic defense. Altogether, our work demonstrates a proof-of-principle of the power of “bottom-up” approaches to reveal the forces determining the fitness of each member of the microbiome as a function of the interaction of parts unpredictable by studying each part alone nor reducible from the sum.

Limitations of the study

There are certain limitations of our work that will be the focus of future research. The first focus will be to understand the significance of glycan-specific impacts on the strain-level fitness of butyrate on the *Bacteroides* within a complex community ecological context such in competition for glycans with butyrate producing bacteria *in vivo*. Secondly, while we find a negative correlation between *Bacteroides* fitness, Acyl-CoA gene expression, and butyrate levels *in vivo*, we do not know the glycan components of the diet or mucosa for each person and how the presence of specific glycans impacts butyrate-associated fitness effects in human cohorts. Relatedly, while we present accumulation of butyryl-CoA as a candidate factor mediating the inhibitory effects of butyrate on the *Bacteroides*, whether and how butyryl-CoA is directly toxic and the molecular mechanisms of butyrate inhibitory functions by sugar and across strains remain to be determined.

Author Manuscript Author Manuscript Author Manuscript Author Manuscript

STAR★METHODS

RESOURCE AVAILABILITY

Lead contact—Requests for further information and resources may be directed to and will be fulfilled by the lead contact, Seth Rakoff-Nahoum (seth.rakoff-nahoum@childrens.harvard.edu).

Materials availability—Plasmids and recombinants strains generated in this study will be distributed without restriction on request.

Data and code availability

- The raw RNA_Seq and Tn_Seq data from this study have been deposited in the NCBI Short-Read Archive (SRA) under the BioProject ID PRJNA640947 (BioSample IDs for RNASeq: SAMN15338436-15338444; BioSample IDs for Tn_Seq data: SAMN15338433-15338435).
- This paper does not report original code.
- Any additional information required to reanalyze the data reported in this paper is available from the lead contact upon request.

EXPERIMENTAL MODEL AND SUBJECT DETAILS

Microbial strains—Bacterial strains used in this study were listed in Key Resource Table. Bacteroidales strains were grown on brain-heart-infusion supplemented with hemin (50 mg/L) and vitamin K_1 (0.25 mg/L) (BHIS) agar plates, in basal medium (BS; proteose peptone (20 g/L), yeast extract (5 g/L), NaCl (5 g/L), glucose (5 g/L), potassium phosphate dibasic (5 g/L), cysteine (0.5 g/L), hemin (50 mg/L) and vitamin K_1 (0.25 mg/L)) (Pantosti et al., 1991), or in minimal media (MM; ammonium sulfate (1 g/L), sodium carbonate (1 g/L), potassium phosphate monobasic (0.9 g/L), sodium chloride (0.9 g/L), calcium chloride dihydrate (26.5 mg/L), magnesium chloride hexahydrate (2 mg/L), manganese(II) chloride tetrahydrate (1 mg/L), cobalt(II) chloride hexahydrate (1 mg/L), hemin (50 mg/L), vitamin K_1 (0.25 mg/L), ferrous sulfate heptahydrate (4 mg/L), vitamin B_{12} (5 mg/L)) with 0.25% glucose, or the indicated sugar as carbon source (Rakoff-Nahoum et al., 2014). Cultures were grown at 37°C in an anaerobic chamber (Coy Laboratory) with 80% nitrogen, 10% CO_2, and 10% hydrogen. *Escherichia coli* was grown in Luria-Burtani (LB) medium, or on LB agar plate. As necessary, antibiotics were added as the following concentrations: ampicillin 100 μg/mL, kanamycin 50 μg/mL, and gentamycin 200 μg/mL for *E. coli*, and erythromycin 5 μg/mL for *Bacteroides* strains. For the inducible promoter, anhydrotetracycline (aTc) was dissolved in 100% ethanol at 2 mg/mL and used at the indicated concentrations (0-25 ng/mL). Isopropyl β-D-1-thiogalactopyranoside (IPTG) was added to culture medium at the final 1 mM, or 0.4 mM concentration.

Animal model—Six week old female germ-free C57BL/6 mice were used for gnotobiotic mouse experiments. Brigham and Women's Hospital Massachusetts Host-Microbiome Center approved under protocol 2020N000054. Mice were housed in Class Biological Isolator in a temperature-controlled (~21°C) facility on a 12 h light/dark cycle. Mice were

Author Manuscript Author Manuscript Author Manuscript Author Manuscript

fed a standard chow (Laboratory Rodent Diet 5025, LabDiet, St. Louis, MO, USA) unless otherwise indicated.

METHOD DETAILS

Culture conditions—For growth assays on solid agar plates, three to five colonies from bacteria grown on BHIS plates were suspended in 100 μL of sterile phosphate buffered saline (PBS) and adjusted to OD_{600}~0.1 using a Microplate spectrophotometer (BioTek, Synergy HTX multi-mode reader). Three μl of bacterial suspension was dotted on the MM agar containing 0.25% sugar and grown at 37°C anaerobically for the indicated days. Sugars used to supplement MM as carbon source include monosaccharides (glucose (Glc), fructose (Fru), mannose (Man), *N*-Acetylglucosamine (GlcNAc), galactose (Gal), arabinose (Ara), xylose (Xyl), fucose (Fuc), Rhamnose (Rha), ribose (Rib), and *N*-Acetylgalactosamine (GalNAc)), disaccharides (maltose (Mal), cellobiose (Cel), sucrose (Suc), and palatinose (Pal)), oligosaccharides (3-sialyllactose (3-SL), lacto-N-neotetraose (LNnT), 2-fucosyllactose (2-FL)), and polysaccharides (pullulan, levan, xylan, xyloglucan, arabinan, arabinogalactan, chondroitin sulfate, inulin, pectin, mannan, and glucomannan). All final concentration of sugars was 0.25%, except levan (0.125%). The sodium form of short chain acids formate, acetate, D- and L-lactate, propionate, malonate, succinate, and butyrate were used at 50 mM concentration. In other experiments the concentration of butyrate was titrated 50 mM down to 0.5 mM. For complex media experiments, a modified version of YCFA (Browne et al., 2016) was used: Casitone (5 g/L), yeast extract (1.25 g/L), $NaHCO_3$ (4 g/L), cysteine (1 g/L), K_2HPO_4 (0.45 g/L), KH_2PO_4 (0.45 g/L), NaCl (0.9 g/L), $MgSO_4{\cdot}7H_2O$ (0.09 g/L), $CaCl_2$ (0.09 g/L), hemin (10 mg/L), vitamin K_1 (0.25 mg/L), ferrous sulfate heptahydrate (4 mg/L), Vitamin Supplement (10 mL/L; ATCC) and Trace Mineral Supplement (ATCC: 10 mL/L). For growth experiments with branched chain amino acids, 1 mM of isoleucine (Ile), leucine (Leu), valine (Val), or the mixture of Ile and Val were added to 0.25% Glc or Gal MM agar. Stock solutions of 100 mM were pH neutralized to ~7.0 with NaOH. The recombinant strains harboring plasmids expressing Acyl-CoA metabolic genes were grown in 0.25% Glc MM agar with erythromycin (5 μg/mL). For all figures except kinetics in Figure 2, day 2 images are shown. Images of bacterial growth were taken using Gel doc system (Bio-Rad) each day.

For growth in liquid MM, bacteria were cultured overnight in BS, diluted 1:10 in fresh BS, grown to mid-log (OD_{600}~0.5), then inoculated into 0.25% sugar MM with 1:50 ratio. MM was pre-reduced in the anaerobic chamber overnight. For growth kinetics, 200 μl of bacterial culture were grown in 96-well flat bottom plates using a microplate spectrophotometer, and OD_{600} was measured at every 30 min for 36 h. To calculate growth rate (k), absorbance readings corresponding to exponential phase (OD_{600}: 0.2-0.6) were fit to a log exponential growth equation (Prism 9). For growth of the recombinant strains harboring plasmids expressing Acyl-CoA transferase genes, bacteria were cultured in BS with erythromycin (5 μg/mL) overnight and inoculated to 0.25% Glc MM containing the same antibiotic with 1: 50 ratio.

Author Manuscript Author Manuscript Author Manuscript Author Manuscript

Culture-seq of defined communities

Community cultivation: Quantification of bacterial strains in community cultivation (referred to as "Culture-Seq") was performed on community cultivation with strains as indicated. Each strain was lifted from BHIS plates, adjusted to OD_{600}~0.2 in sterile PBS, mixed equally, after which 3 μl of the bacterial suspension was dotted on 0.25% sugar MM agar with and without 50 mM butyrate and grown for 2 days. Co-culture samples were prepared in biological and technical duplicates.

Amplicon sequencing of the rpsC gene: To lyse bacteria, the dotted patches were cut from the co-culture plates, suspended in 300 μl of PBS by vertexing (3 min), followed by alkalization in 20 mM KOH at 90°C for 10 min and 70°C for 20 min, and neutralization in 20 mM HCl, 90 mM Tris-HCl and 30 mM KCl. The conserved *rpsC* gene was amplified with the cell lysates as template and the barcoded *rpsC* primers (Table S1) under PCR cycles (98°C 10 s, 60°C 10 s, 72°C 1 min with 25 cycles) using Platinum SuperFi PCR Master Mix (Thermo Fisher Scientific). For Illumina sequencing, the PCR fragments were amplified with index primers I5/I7 (Table S1) under PCR cycles (98°C 10 s, 55°C 10 s, 72°C 30 s with 10 cycles), followed by purification using Zymo DNA Clean and Concentrator Kits (Zymo Research). Libraries were pooled, normalized by qPCR using NEBNext Library Quant Kit for Illumina (New England Biolabs), and subjected to Illumina NextSeq 500 platform generating 150-nt single-end reads (Illumina Inc). Primers are listed in Table S1.

Gnotobiotic mouse experiments—Six week old female germ-free C57BL/6 mice were reared in gnotobiotic isolators. Four days prior to colonization, diets were switched from standard chow to custom glycan-free chow (Bioserv S10004) and drinking water containing either 1% inulin (Beneo) (filter sterilized) or 1% citrus pectin (Sigma) (autoclaved). Animals (n = 5/group) were then gavaged with a 4-member *Bacteroides* community of *B. nordii* CL02T12C05 (*Bn* CL02), *B. ovatus* ATCC 8483 (*Bo* ATCC), *B. salyersiae* DSM 18765 (*Bs* DSM), and *B. caccae* ATCC 43185 (*Bc* ATCC), each at $1x10^9$ CFU in sterile PBS. Four days post colonization, mice were transitioned to the same dietary glycan drinking water (inulin or pectin) supplemented with 150 mM Na butyrate (Smith et al., 2013). Feces was collected daily before and after butyrate supplementation. To determine the impact of butyrate on the relative abundance *in vivo* of each *Bacteroides* member, genomic DNA was extracted from feces using ZymoBIOMICS DNA Miniprep Kit (Zymo Research), and amplicon sequencing of the *rpsC* gene was performed as described above. Significant differences were determined by unpaired two-tailed Student's t test.

RNA-seq of *Bacteroides*—*B. thetaiotaomicron* VPI 5482 (*Bt* VPI,) *B. vulgatus* ATCC 8482 (*Bv* ATCC), and *B. vulgatus* CL09 (*Bv* CL09) were cultured overnight in BS and sub-cultured in 2 mL of MM plus the indicated sugar as described above. At early-log phase (OD_{600}~0.25), bacteria were pulsed with acetate, succinate, butyrate (at final concentration of 50 mM), or water control for 1 h, and harvested (13,000 g, 3 min) for total RNA extraction. Following treatment with 200 μL of TRI reagent (Zymo Research) for 5 min at 50°C, bacteria were frozen in dry ice, and stored at −80°C until use. RNA was extracted using Direct-zol RNA Miniprep Plus Kit (Zymo Research) according to the manufacturer's

Author Manuscript Author Manuscript Author Manuscript Author Manuscript

instructions with on-column DNase I treatment and quantified by the NanoDrop (Thermo Fisher Scientific).

RNA-Seq libraries were constructed using a modified version of the RNAtag-seq protocol (Shishkin et al., 2015) by Microbial 'Omics Core at the Broad Institute of MIT and Harvard. Briefly, 0.5 μg of total RNA was fragmented, depleted of genomic DNA, dephosphorylated, and barcoded. rRNA was depleted by using the Ribo-Zero rRNA Removal Kit (Epicenter). After depletion of rRNA, pools of barcoded RNAs were converted to Illumina cDNA libraries (Zhu et al., 2001). cDNA libraries were sequenced on the Illumina Hiseq2500 platform to generate approximately 5 million paired-end reads per sample by Genomics Platform at the Broad Institute of MIT and Harvard.

Intracellular pH measurement—*Bt* VPI and *Bv* ATCC cultured in BS were grown in 0.25% Glc MM as described above, then at early log-phase (OD_{600}~0.2) were pulsed with 50 mM SCFAs and water as control, and incubated for 1 h. The pH indicator BCECF-AM (Thermo Fisher Scientific) was loaded to the cultures to final 1 μM concentration for 20 min to activate in the cytoplasm. One ml of culture was pelleted (13,000 x g, 3 min), washed and resuspended in 1ml of PBS, and then fluorescence intensity of cells was measured at two excitations, 485 nm and 440 nm with fixed emission at 530 nm using a fluorimeter (Tecan). Intracellular pH was determined by the ratio (485 nm/440 nm) of emission intensities. To generate the standard curve of BCECF-AM, each bacterium grown under the Glc conditions was harvested, washed, and incubated in 50 mM potassium phosphate buffer ranging pH 4.5 to pH 9.0 with each 10 μM ionophore nigericin and valinomycin at room temperature for 5 min (Bio-protocol). The standard curve, plotted with pH and the emission ratio, was fitted with nonlinear regression (Sigmoidal, 4PL) using Prism 9 (GraphPad). Each experiment was performed 3 replicates percondition. Significant differences were determined by paired two-tailed t test.

Propidium iodide (PI) staining and flow cytometry—For PI staining experiments, *Bt* VPI and *Bv* ATCC were grown in 0.25% Glc or Gal MM as described above, then at early log-phase were pulsed with SCFAs and water as control and incubated for 1 h. Bacteria were pelleted (13,000 x g, 3 min), washed, and then incubated in PBS with 10 μg/mL PI (Sigma-Aldrich) at room temperature for 15 min. Following washing with PBS two times, cells were fixed in 1ml of 2% paraformaldehyde (Affymetrix) for flow cytometry.

Flow cytometric measurement was performed on a MoFlo XDP flow cytometer (Beckman Coulter Inc., Miami, FL, USA) equipped with a 488 nm (excitation wavelength of PI) argon laser. 50,000 cells were acquired for the analysis. Three parameters were recorded: forward scatter (FSC), related to cell size, side scatter (SSC), related to cell structure, and red fluorescence (PI), related to cell membrane integrity. FSC, SSC, and fluorescence were collected in a logarithmic scale. For gating strategy, each bacterium was grown to mid exponential phase under in Glc to prepare live cells. To prepare killed bacteria, live cells were heated at 55°C for 5 min. In addition to gating on negative controls without PI staining, the mixture of live and the heat-treated bacteria was used to create PI negative, low and high PI bacterial populations. The results of biological triplicate were shown as percentages

Author Manuscript Author Manuscript Author Manuscript Author Manuscript

of PI-positive subpopulation over total events. Significant differences were determined by paired two-tailed t test.

Measurement of bacterial viability—To measure the effect of butyrate on cell viability, *Bv* ATCC and *Bt* VPI were grown in 0.25% sugar MM as described for PI staining experiments. At early log-phase (OD600: ~0.25), bacteria were pulsed with 20 (Figure S3F) or 50 (Figure 3D) mM butyrate or water as control. Bacteria were collected at 0, 0.5, 1, and 5 h, diluted with PBS, and plated on BHIS agars to determine colony forming unit (CFU)/mL. Each experiment was performed with 3 replicates per condition. Significant differences were determined by paired two-tailed t test.

Acyl-CoA identification and measurement using liquid chromatography coupled with mass spectrometry (LC/MS)—For ^{13}C butyrate tracing experiments, *Bt* VPI, *Bv* ATCC and their isogenic strains were grown in 0.25% Glc as described above. At early log-phase (OD600: ~0.25) cultures were pulsed with 10 mM ^{13}C4 butyrate (Cambridge Isotope Laboratories) or water as control and incubated for 30 min. To determine abundance of Acyl-CoAs at steady state, bacteria were pulsed with 20 mM butyrate or water and incubated for 30 min. Five ml cultures of bacteria were harvested (4,000 rpm, 10 min) at 4°C, washed with PBS two times, and pellets stored at −80°C until further use.

For LC/MS analysis, the bacterial pellet was dissolved into 300 μL of 80% MeOH and treated with Sonifier® Cell Disruptor for 1 min. The homogenized solution was centrifuged at 4,350 rpm for 10 min, and the upper clear supernatant was filtered through a 0.2 μm PTFE filter vial. Q Exactive mass spectrometry (Thermo Fisher Scientific) with a UHPLC system (Ultimate 3000) equipped with a 150 mm C18 column (Kinetex® 2.6 μm C18 100 Å LC Column 150 × 3 mm) was used to analyze the samples. The LC/MS method used for detecting Acyl-CoAs was adopted from previous literature (Liu et al., 2015). The following LC program was used: Buffer A: water with 5 mM ammonium acetate; Buffer B: methanol. 0 min: 2% B, 1.5 min: 2% B, 3 min: 15% B, 5.5 min: 95% B, 14.5 min: 95% B, 15 min: 2% B, 20 min: 2% B. Flow speed was 0.5 mL/min. Injection volume was 2 μl. Column temperature was set at 25°C. Mass spec acquisition windows were set to 0-10 min at full MS positive mode. The following parameters were used for data collection: Resolution: 70,000, AGC target: 3e6, Maximum IT: 250 ms, scan range: 700 to 1100 m/z. The data analysis was completed using Thermo Freestyle (Version 1.6) and Qual Browser software (Version 4.3). In the run using various Acyl-CoA standards, all the Acyl-CoAs were detected as $[M+H]^+$ formula. Therefore, we searched Acyl-CoA peaks in samples using $[M+H]^+$ formula for each Acyl-CoA at 5 decimal and 5 ppm resolution. The peak area quantification was done using Genesis method at Freestyle software. The peak area for each sample was then normalized by cell density at OD_{600}.

Quantitative RT-PCR (qRT-PCR)—To measure total transcript levels of CoA transferase gene, *Bt* VPI and *Bv* ATCC cultivated BS were subcultured in 0.25% sugar MM as described above, collected at early-log (OD_{600}~0.2), mid-log (OD_{600}~0.4), and late-log phases (OD_{600}~0.6). For RNA extraction of the recombinant strains harboring plasmids expressing CoA transferase genes, bacteria were grown in 0.25% sugar MM with

Author Manuscript Author Manuscript Author Manuscript Author Manuscript

erythromycin late exponential phase (Figures 6G and 6I). After pelleting (13,000 x g, 3 min), bacteria were treatment with Trizol for 5 min, then, total RNA was extracted according to Direct-zol RNA Miniprep Plus Kit (Zymo Research) protocol.

cDNA of 200 ng RNA was synthesized using SuperScript VI (Thermo Fisher Scientific) according to the manufacturer's instructions. Quantification of transcripts was performed by real-time PCR (QuantStudio 3) using Fast SYBR Green Master Mix (Applied Biosystems). mRNA levels of target genes were normalized to 200-fold dilution of 16S rRNA *rrs* gene abundance. The relative amount of each PCR product was calculated from standard curves obtained from PCRs with the same primers and serially diluted genomic DNA as templates. The BVU_1163, BT_3193, and *rrs* genes were detected using primer pairs 114/115, 126/127, and 110/111, respectively. The list of primers used for qRT-PCR is presented in Table S1.

Construction of *Bacteroides* transposon mutant library—The transposon plasmid pSAM_BcellWH2 (Wu et al., 2015) was modified by adding back the *rrnB* terminator sequences to the downstream region of *ermG* within the transposon to reduce the potential polar effect derived by the strong promoter of the *ermG* gene, named as pWH2-Term6. For conjugation, *Bacteroides* strains were grown in 20 mL of BS media to early-lag phase culture (OD_{600} < 0.1). The *E. coli* S17-1 λ *pir* (Simon et al., 1983) donor harboring pWH2-Term6 was grown in 1 mL of LB media to log phase. Harvested bacteria were mixed, spotted on BHIS agar plate, and incubated at 37°C less than 18 h aerobically. After pooling the conjugation reaction, Tn mutants were selected on BHIS agar supplemented with gentamicin (200 μg/mL) and erythromycin (5 μg/mL) anaerobically at 37°C for 48 h. Approximately, 100,000 colonies were pooled in LB supplemented with 25% glycerol, and stored at −80°C.

Transposon sequencing (Tn-seq) of *Bacteroides* Tn mutants—An aliquot of the transposon mutant bank was thawed, recovered overnight in BS (starting OD_{600}~0.1), back diluted 1:10 to fresh BS, and grown to mid-log phase (OD_{600}~0.5) in duplicate. This culture (an aliquot was saved as input control) was then diluted 50-fold in 2 mL of MM containing 0.25% defined sugar with and without 50 mM butyrate and grown to mid-log phase at 37°C under anaerobic conditions.

To construct Tn-seq libraries for sequencing, the collected samples were first subjected to DNA extraction using Invitrogen PureLink Genomic DNA mini kit (Thermo Fisher Scientific). An aliquot of 5 μg of DNA was sheared in 100 μL water to 300~500 bp using a M220 focused ultrasonicator (Covaris Inc). The sheared DNA was subjected to end repair, A-tailing, and ligated with prepared adapters (generated by annealing two oligos: 5¢-TACCACGACCA-NH2-3¢ and 5¢-GTGACTGGAGTTCAGACGTGTGCTCTTCCGATCTGGTCGTGGTAT-3¢) using NEBNext Ultra DNA Library Prep Kit (New England Biolabs). Next, transposon junction fragments containing the insertion sites were enriched by two PCR steps using Platinum SuperFi PCR Master Mix (Thermo Fisher Scientific). In the first PCR, the fragments were amplified (98°C 10 s, 60°C 10 s, 72°C 30 s with 25 cycles) with universal primers matching the transposon and adaptor sequence (Table S1). In the second PCR, the PCR products

Author Manuscript Author Manuscript Author Manuscript Author Manuscript

were amplified (98°C 10 s, 60°C 10 s, 72°C 30 s with 18 cycles) with Truseq-compatible indexed primers containing specific annealing sequences (Table S1). The PCR fragments corresponding to 200~600 bp were selected using AMPure XP beads (Beckman Coulter Inc). These libraries were normalized using NEBNext Library Quant kit (New England Biolabs) and subjected to NextSeq500 High Output sequencing (Illumina Inc).

Construction of strains—To delete target loci by allelic replacement, first, we modified the suicide vector pKNOCK-*bla-erm*Gb (Koropatkin et al., 2008) with a counter-selection system mediated by a variant phenylalanyl-tRNA synthetase ($PheS_{A303G}$), lethal in the presence of 4-chlorophenylalanine (Kino et al., 2016). Briefly, the *pheS* gene, along with its native promoter, was PCR amplified with genomic DNA of *Bacteroides fragilis* as template and two primer sets (Table S1) generating the mutated *pheS* gene (*pheS**). The PCR fragments were cloned into the MfeI site of pKNOCK-*bla-erm*Gb using GeneArt Seamless Cloning and Assembly Enzyme Kit (Thermo Fisher Scientific), resulting in a counterselection plasmid pKNOCK-*bla-erm*Gb_*phe*S*.

For deletion of BT_3942 in *Bt* VPI, BVU_1163, BVU_0574, or BVU_2719 in *Bv* ATCC, and the homolog genes of BVU_1163, or BVU_2719 in *Bv* CL09, approximately, 1 kb upstream and downstream flanking regions of the deletion locus were PCR-amplified, cloned into pKNOCK-*bla-erm*Gb_*phe*S* digested BamHI with ClaI using GeneArt Seamless Cloning and Assembly Enzyme Kit, and transformed into *E. coli* DH5a λ *pir* (Pal et al., 2005). The plasmid DNA was transferred into *Bacteroides* strains by triparental mating using *E. coli* carrying the helper plasmid RK231 at 37°C aerobically, and merodiploid *Bacteroides* cells were selected on BHIS plates with gentamicin (200 μg/mL) and erythromycin (5 mg/mL) anaerobically at 37°C. Resistant colonies were restreaked on BHIS plates with erythromycin and grown anaerobically at 37°C for 2 days. For counterselection, the isolated strains were streaked on 0.25% glucose MM containing 4-chloro-phenylalanine (2 mg/mL) and incubated anaerobically for 3-4 days. The deletion of target genes was confirmed with primers corresponding to upstream and downstream flanking regions. Deletion strains and primers for the deletion constructs were listed in Key Resources Table and Table S1.

For inducible promoter-derived expression of the BVU_1163 gene, *Bv* ATCC isogenic strains were constructed as follows: open reading frame of BVU_1163 was amplified with primers 259/147 and genomic DNA of *Bv* ATCC as template and cloned into the *Bacteroides* species integrative plasmid pNBU2-*erm*_TetR-p1T_DP-GH023 containing the engineered inducible promoter(Lim et al., 2017) digested with NcoI and ClaI. Then, *Bv Δ1163* and *Bv Δ1163 Δ0574* strains were conjugated by *E. coli* carrying the integration plasmid and selected on BHIS plates with gentamicin (200 μg/mL) and erythromycin (5 μg/mL).

Construction of plasmids

Heterologous expression of Acyl-CoA thioesterases: Plasmid pBT_3942 and pBVU_0767 were constructed as follows: Open reading frames (ORF), including ~50 bp of upstream of the gene to capture native ribosomal binding site (RBS) of BT_3942 and BVU_0767,

Author Manuscript Author Manuscript Author Manuscript Author Manuscript

were amplified with primers 190/191 and genomic DNA of *Bt* VPI as template, and primers 192/193 and genomic DNA of *Bv* ATCC as template, respectively, using Platinum SuperFi PCR Master Mix. The PCR fragments were digested with BamHI and KpnI and cloned into the *Bacteroides* expression plasmid pFD340 harboring constitutive promoter digested with the same restriction sites (Smith et al., 1992).

Promoter swapping: The CoA transferase genes BVU_1163 and BT_3193 appeared to form an operon with the upstream genes BVU_1164 and BT_3193a, respectively (Figure S5C). Consistent with this, putative RNA polymerase binding sites were found upstream regions of the BVU_1164 and BT_3193a genes (Figure 6H). For promoter swapping of the CoA transferase genes, 220 bp and 200 bp upstream of the start codons of the BVU_1164 and BT_3193a genes were used for the promoter regions p*Bv* and p*Bt*, respectively. The ORF regions of the BVU_1163 and BT_3193 genes were designed to include their own native RBS (~50 bp upstream of the gene).

For plasmids p*Bv*_1163 and p*Bt*_1163, the promoter regions p*Bv* and p*Bt* were generated with primers 208/71 and genomic DNA of *Bv* ATCC as template, and primers 132/136 and genomic DNA of *Bt* VPI as template, respectively. ORFs of BVU_1163 were generated with primer sets 70/72 for the p*Bv* promoter, and 135/72 for the p*Bt* promoter and genomic DNA of *Bv* ATCC, respectively. The two fragments corresponding to the promoter and ORF regions were assembled into promoterless-pFD340, of which IS*4351* promoter was removed by digestion with SphI and KpnI, using GeneArt Seamless Cloning and Assembly Enzyme Kit.

For plasmids p*Bv*_3193 and p*Bt*_3193, the promoter regions p*Bv* and p*Bt* were generated with primers 208/75 and genomic DNA of *Bv* ATCC, and primers 132/131 and genomic DNA of *Bt* VPI, respectively, and ORFs of BT_3193 were generated with primer sets 74/77 for the p*Bv* promoter, and 130/77 for the p*Bt* promoter and *Bt* VPI genomic DNA, respectively. The two fragments corresponding to the promoter and ORF regions were assembled into promoterless-pFD340 as described above.

For control vectors, pN_1163 and pN_3193, ORFs of BVU_1163 and BT_3193 were generated with primers 142/57 and genomic DNA of *Bv* ATCC, and primers 143/77 and genomic DNAof *Bt* VPI, respectively, and cloned into promoterless pFD340 digested with SphI and KpnI.

To examine expression level of CoA transferase proteins, plasmids p*Bv*_1163-HA and p*Bt*_3193-HA were constructed as follows: Plasmid p*Bv*_1163 and p*Bt*_3193 as template was amplified with primers 208/477 and 132/478, respectively, then the PCR fragments inserting HA tag were cloned into promoterless pFD340 digested with SphI and KpnI.

Nucleotide polymorphisms within −33 promoter region: Derivatives of plasmid p*Bv*_1163 with nucleotide substitutions in −33 region (TTTA) of the BVU_1163 promoter were constructed with plasmid p*Bv*_1163 as template and the following primer pairs: primers 208/214 and 213/72 for p*Bv*_TTAG-1163 (promoter polymorphism); primers 208/212 and 211/72 for p*Bv*_TTAG_down-1163 (polymorphism location: deletion of TAGA

Author Manuscript Author Manuscript Author Manuscript Author Manuscript

in the downstream region of TTTA). The PCR fragments were assembled with promoterless pFD340 digested with restriction enzymes SphI and KpnI using GeneArt Seamless Cloning and Assembly Enzyme Kit.

Derivatives of plasmid p*Bt*_1163 with nucleotide substitutions in −33 region (TTAG) of the BT_3193 promoter were constructed with plasmid p*Bt*_1163 as template and the following primer pairs: primers 132/216 and 215/72 for p*Bt*_TTTA-1163 (promoter polymorphism); primers 132/324 and 323/72 for p*Bt*_TTTA_up-1163 (polymorphism location: insertion of TTTA in the upstream region of TTAG, and replacement of TTAG with AATC). The PCR fragments were assembled with promoterless pFD340 digested with restriction enzymes SphI and KpnI using GeneArt Seamless Cloning and Assembly Enzyme Kit.

Sequence analysis confirmed that the plasmids had the expected nucleotide sequences. The list of primers used in this study is presented in Table S1.

Expression, purification, and activity of recombinant Acyl-CoA thioesterase and Acyl-CoA transferase enzymes—Acyl-CoA thioesterase BT_3942 and BVU_0767 genes, and Acyl-CoA transferase BVU_1163 gene were amplified with primers (Table S1) and genomic DNA of *Bt* VPI and *Bv* ATCC 8482 as template, respectively, and cloned into the pET-28a (Novagen) digested with NcoI and AvaI using GeneArt Seamless Cloning and Assembly Enzyme Kit. The recombinant plasmids were transformed into *E. coli* BL21 (DE3) (Novagen) strains, grown to OD_{600}~0.5 in LB plus kanamycin at 37°C and induced by 1 mM of IPTG at 15°C for 4 h (BT_3942), or by 0.4 mM of IPTG at 15°C overnight (BVU_0767, BVU_1163). After harvesting (6000 g, 10 min, 4°C), cells were suspended in lysis buffer (50 mM Tris-HCl (pH 8.0), 150 mM NaCl, 1.0 mM Imidazole) with protease inhibitor (Halt Protease Inhibitor Cocktail, Thermo Fisher Scientific) and lysed by sonication. The cell extracts were spun down, filtered through a 0.45 μm filter, mixed with 2 mL of pre-washed Ni-NTA resin (HisPur Ni-NTA Resin, Thermo Fisher Scientific), and incubated on a rotator at 4°C for 1 h. The resin was loaded onto a column and washed with lysis buffer containing 25 mM Imidazole. The recombinant proteins were eluted using lysis buffer containing 250 mM Imidazole for BT_3942, or 300 mM Imidazole for BVU_0767 and BVU_1163. After concentration in a spin concentrator pre-dialysis, fractions of each protein were dialyzed overnight at 4°C in 1 L of storage buffer (50 mM Tris-HCl (pH 8.0), 150 mM NaCl, 10% glycerol) in three times. The size and purity of the recombinant proteins were verified by SDS-PAGE gel (NuPAGE 4 to 12%, Bis-Tris Mini Protein Gel, Thermo Fisher Scientific), and the concentration of each protein was measured by absorbance at 280 nm using Nanodrop (Thermo Fisher Scientific).

Acyl-CoA thioesterase activity of the recombinant proteins was determined spectrophotometrically at 412 nm with 5,5¢-dithiobis (2-nitrobenzoic acid) (DTNB) as previously reported with minor modification (Jawed et al., 2016). All reactions were carried out 200 μl of 60 mM potassium phosphate buffer (pH 7.4) containing 200 μM DTNB, 5 μM bovine serum albumin, and 100 μM of different chain length of acyl-CoAs (acetyl-CoA, propionyl-CoA, butyryl-CoA, hexanoyl-CoA, decanoyl-CoA and palmitoyl-CoA) in 96-well plate. The reaction was initiated by adding 5 μl of the recombinant enzyme at final concentration 25 nM into the mixture at 37°C. The liberation of free CoA was

Author Manuscript Author Manuscript Author Manuscript Author Manuscript

monitored at 412 nm for 25 min using a microplate spectrophotometer. Enzymatic assays were performed with duplicates per condition. Significant differences were determined by unpaired two-tailed t test.

Acyl-CoA transferase activity of the recombinant protein was measured by determining the concentrations of acetyl-CoA with citrate synthase assay as previously reported with minor modifications (Sato et al., 2016). Briefly, the reaction mixture (40 μl) consisted of 40 mM potassium phosphate buffer (pH 8.0), 100 mM sodium acetate, and 0.5 mM of different chain lengths of acyl-CoAs (propionyl-CoA, butyryl-CoA, succinyl-CoA, and hexanoyl-CoA). The purified enzyme was added to the reaction mixture at final concentration 1.5 μM and incubated for 5 min at 37°C. The reactions were terminated by the addition of 10 μl of 4.5% trichloroacetic acid and neutralized by adding 25 μL of 400 mM potassium phosphate buffer (pH 8.0). To determine acetyl-CoA, assay mixture (25 μl) containing 4 mM oxaloacetate, 4 mM DTNB, and 36.8 μg/mL citrate synthase was added to the reaction mixture, and incubated at 37°C for 30 min. The free CoA of the reaction mixture was measured at 412 nm using a microplate spectrophotometer. Enzymatic assays were performed with duplicates per condition.

Western blot assay of Acyl-CoA transferases—To examine expression of Acyl-CoA transferase in protein level, *Bt* and *Bv* strains harboring plasmids p*Bt*_3193-HA and p*Bv*_1163-HA were grown in 0.25% Glc as described above, and harvested (12,000 rpm x 5 min) at early and late log phase. Bacteria were suspended in PBS with protease inhibitor and lysed by sonication. Cell extracts (30 μg-150 μg protein) were loaded on 4 to 12% NuPAGE gel (Thermo Fisher Scientific) and then transferred to nitrocellulose membrane. Membranes were blocked with 3% skim milk solution at room temperature for 30 min. Primary antibody, mouse anti-HA (Santa Cruz) and mouse anti-*E. coli* RpoA (Biolegend), which cross-reacts with *Bacteroides* RpoA (Hecht et al., 2017), were used at 1:4000 dilution in PBST (PBS/0.05% Tween 20) with 1% skim milk. Secondary horseradish peroxidase-conjugated anti-mouse antisera (Santa Cruz) was used at 1:5,000 dilution. Blots were developed with SuperSignalWest Femto Maximum Sensitivity Substrate (Thermo Fisher Scientific).

QUANTIFICATION AND STATISTICAL ANALYSIS

Phylogenetic tree—The phylogenic tree of Bacteroidales strains was generated (Figure 2A), based on the core genes (526 for Bacteroides and 1114 for Parabacteroides) which have 80% identity in amino acid sequence levels, using the concatenated alignment for a neighbor-joining tree in MEGA (https://www.megasoftware.net/).

Analysis of fitness effects of butyrate across strains and sugars—53 Bacteroidales strains were grown on MM agar plates under 11 monosaccharides conditions in the presence and absence of butyrate for 4 days. To calculate butyrate susceptibility across strains and sugars (Figure 2A), the images of bacterial growth over time were analyzed using a custom built MATLAB (MatWorks) script. First, the location of the focal colony was automatically detected (with manual checking and adjustment if necessary) using the *CircularHough_Grd* function, and the average pixel density across the colony was used as a quantitative growth measurement, normalized by the maximum pixel density in control

Author Manuscript Author Manuscript Author Manuscript Author Manuscript

conditions. For ease of interpretation, we then discretely binned these normalized values so that growth on a given day can vary between 0 (no growth) or 5 (pixel density equal to or above maximum value in control conditions). This process yielded two 1 × 4 vectors of discrete values that describe the growth over time of the focal strain, in the focal sugar, either with or without butyrate. Inhibition level on each day was calculated by subtracting the butyrate growth vector from the control vector (note, we set any negative values to zero, these correspond to instances where the focal strain grew more with butyrate than without). The inhibition score was defined as the sum of this inhibition vector across strains and sugars, creating a matrix that describes the level of inhibition across all conditions.

Culture-seq data analysis—Illumina raw reads were first demultiplexed using skewer v0.2.2 (Lim et al., 2017) allowing no mismatch with both primers, next quality trimmed using vsearch v2.7.1 (Rognes et al., 2016) with the setting "–fastq_filter-fastq_truncee 1," and further trimmed to the uniform length 110 nt. The trimmed reads were dereplicated and finally used to map against a custom database of *Bacteroides rpsC* sequences using vsearch with the "–usearch_global" setting. Chimeras were removed using usearch v10.0.240 (Edgar, 2010).

RNA-seq data analysis—Sequencing reads from each sample in a pool were demultiplexed based on their associated barcode sequence using custom scripts. Reads were aligned to the *B. thetaiotaomicron* VPI 5482, *B. vulgatus* ATCC 8482, and *B. vulgatus* CL09 reference genomes using BWA (Li and Durbin, 2009) and read counts were assigned to genes and other genomic features using custom scripts. Differential expression analysis was conducted with DESeq2 (Love et al., 2014).

Pairwise comparisons were performed with log2-transformed normalized RNA-seq reads between SCFAs and water control in different sugars with biological duplicates per condition. To identify genes expression that correlated with the strength of butyrate fitness effects, expression of statistically significant genes ($|\log2(\text{fold change})| > 1$, $\text{padj} < 0.05$) with 1.5 fold difference across sugars were grouped as follows: 1) Glc < GlcNAc < Gal or Xyl, 2) Glc > GlcNAc > Gal or Xyl, 3) Glc > GlcNAc = Gal = Xyl, or 4) Glc < GlcNAc = Gal = Xyl, and no gradient across 4 sugars (Glc = GlcNAc = Gal = Xyl). RNA-Seq data were listed in Table S2.

Functional annotation term and/or clustering of butyrate-responding genes was analyzed by using DAVID 6.8 (NIAID/NIH), and statistically significant functional groups were highlighted in color ($p_{val} < 0.001$).

Tn-seq data analysis—To analyze the fitness of transposon mutants in the library, Illumina raw reads were subjected to the following bioinformatics pipeline. The demultiplexed reads were first trimmed using cutadapt v1.17 (Martin, 2011) to remove transposon and adaptor sequences ("-gGACTTATCATCCAACCTGT -O 17 -e 0.2" and "-aATACCACGAC -O 5 -e 0.1 -m 15"). These trimmed reads were then mapped to the corresponding *Bacteroides* reference genome using Bowtie v1.2.2 (Langmead et al., 2009) with the setting "-n 3 -l 28 -e 120–best." The derived insertion tallies were subjected to comparative analysis between each pair of control and butyrate samples using Transit v2.1.0

Author Manuscript Author Manuscript Author Manuscript Author Manuscript

(DeJesus et al., 2015) under the "resampling" mode with the setting "-n TTR -iN 0.05 -iC 0.05." As each experiment was performed in biological duplicates, to combine fold change (butyrate /control) and *p*-values from two replicates, we used the smaller absolute value fold change and the higher *p*-value for each gene, which is more conservative than other methods such as Fisher's method. As the Transit resampling method had a default *p*-value detection limit of 10e-4, for more significant hits that were marked as *p*-value = 0, we randomly assigned *p*-values < 10e-4 for the sake of volcano plots. Statistically significant genes were highlighted in red (|log2(fold change)|> 1, $p_{adj} < 0.05$) in volcano plots.

Tn-Seq data were listed in Table S3.

HMP2 data analysis—Functional profiles for metagenomes (MGX), metatranscriptomes (MTX) and metabolomes (MBX) were downloaded from the Inflammatory Bowel Disease Multi'omics Databases (https://www.ibdmdb.org/) (Lloyd-Price et al., 2019) on April 2019. These included 1,638 MGX, 818 MTX and 546 MBX samples, respectively, in total comprising 132 subjects (with multiple time points for each). The abundance profiles of gene families (UniRef90s) (Suzek et al., 2007) for MGX and MTX were generated by HUMAnN 2.11.0, which we previously optimized to identify and quantify genes from individual microbial species present at > 1x fold-coverage in a community sequencing sample (Franzosa et al., 2018). Gene expression profiles were analyzed as the ratios between each gene family's MTX versus MGX abundance per sample, where undefined values (zero divided by zero) and non-finite values (non-zero divided by zero) were removed (treated as NA). Metabolomic profiles were measured using a combination of four LC-MS method (Lloyd-Price et al., 2019). The sum-normalized metabolite data (sum-normalized to 1 per sample per LC-MS method) and median-normalized metabolite counts (which is used to reduce technical sample to sample variation) were taken from the associated publication's supporting information (Lloyd-Price et al., 2019). Both types of metabolite data were analyzed, with roughly equivalent results (Figure S6A). MGX, MTX and MBX samples were strictly matched for multi-omic association if they derived from the same subject and sampling time point (yielding 88 samples from 26 nonIBD participants: 52 samples from 14 adult participants and 36 samples from 12 child participants). Since multiple samples from the same subject were often present, we considered only the last matched MGX:MTX:MBX samples from each subject for the following correlation analysis (yielding 26 samples from 26 individuals) (Table S5). For Figure 7B, the relative abundance range for low butyrate level (minimum to median value) is 3.56×10^{-5} to $2.15 \times 10^{\sim 3}$; for high-butyrate (median to maximum value) is 2.15 × 10-3 to 9.67×10^{-3}.

To explore putative associations between microbial features and metabolites in *Bacteroides* CoA metabolism pathway genes, we identified CoA transferase (BVU_1163) homologs in *Bacteroides* using a UniRef-based protein sequence catalog (Suzek et al., 2015) (UniRef release 2014_07). We first: i) identified the gene family UniRef90_R7P442 (UniRef90 cluster: > 90% amino acid identity and > 80% coverage) of BVU_1163, then ii) linked this to its corresponding UniRef50 cluster UniRef50_P52043 (requiring >50% identity and > 80% coverage), iii) summed the gene abundances of all UniRef90s in this UniRef50 cluster per sample, and finally iv) further summed the abundances of all such UniRef50 clusters (members of UniRef50_P52043) from *Bacteroides* species per sample. Two butyrate

Author Manuscript Author Manuscript Author Manuscript Author Manuscript

levels (low-butyrate and high-butyrate) were defined as being above or below the median metabolomic abundance of butyrate (across all included samples, Table S5). Within each of these two butyrate levels, we calculated the Spearman correlation between the gene abundance and gene expression contributed by BVU_1163 *Bacteroides* UniRef50 families. The same approach was then applied to succinate metabolite abundances as well.

BLAST alignment—Amino acid sequence alignment of Acyl-CoA thioesterase BT_3942 from *Bt* VPI as reference and Acyl-CoA transferase BVU_1163 from *Bv* ATCC as reference was performed using NCBI BLAST service against 42 *Bacteroides* strains (Figure S5).

Other statistical analyses—Images of bacterial growth are one representative of at least biological duplicates or triplicates. Graphpad Prism version 9 was used for all statistical analyses. For pairwise and two independent group comparison Student's t test was used, while for multiple group comparison Two-way ANOVA were performed. Statistical significance is indicated as follows: ns > 0.05, *p < 0.05, **p < 0.01, ***p < 0.001, ****p < 0.0001. Error bars represent the standard error of the mean. For correlation analysis of MGX:MTX:MBX samples, correction for multiple hypothesis testing was performed using a Benjamini-Hochberg false discovery rate (FDR) approach with a conservative FDR q-value < 0.05 required as a threshold for statistical significance.

Supplementary Material

Refer to Web version on PubMed Central for supplementary material.

ACKNOWLEDGMENTS

We thank members of the S.R.-N. lab for helpful comments on the manuscript, Beneo (Inulin) and Glycom (HMO) for reagents, and J. Livny and the Broad MOC (assistance for RNASeq). We thank M. and B. Rakoff-O'Neill for sugar preparation and tube labelling. This work is supported by NIDDK R24DK110499 (C.H.), Keck Foundation (J.-K.W.), Mathers Foundation (J.-K.W., S.R.-N.), a NDSEG Fellowship (G.A.K.), a Sir Henry Wellcome Postdoctoral Research Fellowship (K.Z.C.), the Harvard Digestive Disease Center (P30 DK034854 to S.R.-N.), a Career Award for Medical Scientists from the Burroughs Wellcome Fund (S.R.-N.), a Pew Biomedical Scholarship (S.R.-N.), a Basil O'Connor Starter Scholar Award from the March of Dimes (S.R.-N.), and the NIH (1K08AI130392-01 and DP2GM136652 to S.R.-N.).

REFERENCES

Arumugam M, Raes J, Pelletier E, Le Paslier D, Yamada T, Mende DR, Fernandes GR, Tap J, Bruls T, Batto J-M, et al. ; MetaHIT Consortium (2011). Enterotypes of the human gut microbiome. Nature 473, 174–180. [PubMed: 21508958]

Babicki S, Arndt D, Marcu A, Liang Y, Grant JR, Maciejewski A, and Wishart DS (2016). Heatmapper: web-enabled heat mapping for all. Nucleic Acids Res. 44, W147–W153. [PubMed: 27190236]

Barcik W, Boutin RCT, Sokolowska M, and Finlay BB (2020). The Role of Lung and Gut Microbiota in the Pathology of Asthma. Immunity 52, 241–255. [PubMed: 32075727]

Bayley DP, Rocha ER, and Smith CJ (2000). Analysis of cepA and other Bacteroides fragilis genes reveals a unique promoter structure. FEMS Microbiol. Lett 193, 149–154. [PubMed: 11094294]

Belkaid Y, and Harrison OJ (2017). Homeostatic Immunity and the Microbiota. Immunity 46, 562–576. [PubMed: 28423337]

Author Manuscript Author Manuscript Author Manuscript Author Manuscript

Browne HP, Forster SC, Anonye BO, Kumar N, Neville BA, Stares MD, Goulding D, and Lawley TD (2016). Culturing of 'unculturable' human microbiota reveals novel taxa and extensive sporulation. Nature 533, 543–546. [PubMed: 27144353]

Charbonneau MR, Blanton LV, DiGiulio DB, Relman DA, Lebrilla CB, Mills DA, and Gordon JI (2016). A microbial perspective of human developmental biology. Nature 535, 48–55. [PubMed: 27383979]

Coyne MJ, Roelofs KG, and Comstock LE (2016). Type VI secretion systems of human gut Bacteroidales segregate into three genetic architectures, two of which are contained on mobile genetic elements. BMC Genomics 17, 58. [PubMed: 26768901]

Cummings JH, Pomare EW, Branch WJ, Naylor CP, and Macfarlane GT (1987). Short chain fatty acids in human large intestine, portal, hepatic and venous blood. Gut 28, 1221–1227. [PubMed: 3678950]

DeJesus MA, Ambadipudi C, Baker R, Sassetti C, and Ioerger TR (2015). TRANSIT–A Software Tool for Himar1 TnSeq Analysis. PLoS Comput. Biol 11, e1004401. [PubMed: 26447887]

Donia MS, and Fischbach MA (2015). HUMAN MICROBIOTA. Small molecules from the human microbiota. Science 349, 1254766. [PubMed: 26206939]

Eckburg PB, Bik EM, Bernstein CN, Purdom E, Dethlefsen L, Sargent M, Gill SR, Nelson KE, and Relman DA (2005). Diversity of the human intestinal microbial flora. Science 308, 1635–1638. [PubMed: 15831718]

Edgar RC (2010). Search and clustering orders of magnitude faster than BLAST. Bioinformatics 26, 2460–2461. [PubMed: 20709691]

Elinav E, Garrett WS, Trinchieri G, and Wargo J (2019). The cancer microbiome. Nat. Rev. Cancer 19, 371–376. [PubMed: 31186547]

Ferreiro A, Crook N, Gasparrini AJ, and Dantas G (2018). Multiscale Evolutionary Dynamics of Host-Associated Microbiomes. Cell 172, 1216–1227. [PubMed: 29522743]

Fischbach MA, and Sonnenburg JL (2011). Eating for two: how metabolism establishes interspecies interactions in the gut. Cell Host Microbe 10, 336–347. [PubMed: 22018234]

Foster KR, Schluter J, Coyte KZ, and Rakoff-Nahoum S (2017). The evolution of the host microbiome as an ecosystem on a leash. Nature 548, 43–51. [PubMed: 28770836]

Franzosa EA, McIver LJ, Rahnavard G, Thompson LR, Schirmer M, Weingart G, Lipson KS, Knight R, Caporaso JG, Segata N, and Huttenhower C (2018). Species-level functional profiling of metagenomes and metatranscriptomes. Nat. Methods 15, 962–968. [PubMed: 30377376]

Greenblum S, Carr R, and Borenstein E (2015). Extensive strain-level copy-number variation across human gut microbiome species. Cell 160, 583–594. [PubMed: 25640238]

Hagan T, Cortese M, Rouphael N, Boudreau C, Linde C, Maddur MS, Das J, Wang H, Guthmiller J, Zheng N-Y, et al. (2019). Antibiotics-Driven Gut Microbiome Perturbation Alters Immunity to Vaccines in Humans. Cell 178, 1313–1328.e13. [PubMed: 31491384]

Hecht AL, Casterline BW, Choi VM, and Bubeck Wardenburg J (2017). A Two-Component System Regulates Bacteroides fragilis Toxin to Maintain Intestinal Homeostasis and Prevent Lethal Disease. Cell Host Microbe 22, 443–448.e5. [PubMed: 28943327]

Honda K, and Littman DR (2016). The microbiota in adaptive immune homeostasis and disease. Nature 535, 75–84. [PubMed: 27383982]

Huang DW, Sherman BT, and Lempicki RA (2009). Systematic and integrative analysis of large gene lists using DAVID bioinformatics resources. Nat. Protoc 4, 44–57. [PubMed: 19131956]

Integrative HMP (iHMP) Research Network Consortium (2019). The Integrative Human Microbiome Project. Nature 569, 641–648. [PubMed: 31142853]

Jacobson A, Lam L, Rajendram M, Tamburini F, Honeycutt J, Pham T, Van Treuren W, Pruss K, Stabler SR, Lugo K, et al. (2018). A Gut Commensal-Produced Metabolite Mediates Colonization Resistance to Salmonella Infection. Cell Host Microbe 24, 296–307.e7. [PubMed: 30057174]

Jawed K, Mattam AJ, Fatma Z, Wajid S, Abdin MZ, and Yazdani SS (2016).Engineered Production of Short Chain Fatty Acid in Escherichia coli Using Fatty Acid Synthesis Pathway. PLoS ONE 11, e0160035. [PubMed: 27466817]

Kaiser JC, and Heinrichs DE (2018). Branching Out: Alterations in Bacterial Physiology and Virulence Due to Branched-Chain Amino Acid Deprivation. MBio 9, e01188–18. [PubMed: 30181248]

Author Manuscript Author Manuscript Author Manuscript Author Manuscript

Kannan G, Wilks JC, Fitzgerald DM, Jones BD, Bondurant SS, and Slonczewski JL (2008). Rapid acid treatment of Escherichia coli: transcriptomic response and recovery. BMC Microbiol. 8, 37. [PubMed: 18302792]

Kino Y, Nakayama-Imaohji H, Fujita M, Tada A, Yoneda S, Murakami K, Hashimoto M, Hayashi T, Okazaki K, and Kuwahara T (2016). Counterselection employing mutated pheS for markerless genetic deletion in Bacteroides species. Anaerobe 42, 81–88. [PubMed: 27639596]

Koh A, De Vadder F, Kovatcheva-Datchary P, and Bäckhed F (2016). From Dietary Fiber to Host Physiology: Short-Chain Fatty Acids as Key Bacterial Metabolites. Cell 165, 1332–1345. [PubMed: 27259147]

Kolodziejczyk AA, Zheng D, and Elinav E (2019). Diet-microbiota interactions and personalized nutrition. Nat. Rev. Microbiol 17, 742–753. [PubMed: 31541197]

Koppel N, Maini Rekdal V, and Balskus EP (2017). Chemical transformation of xenobiotics by the human gut microbiota. Science 356, eaag2770. [PubMed: 28642381]

Koropatkin NM, Martens EC, Gordon JI, and Smith TJ (2008). Starch catabolism by a prominent human gut symbiont is directed bythe recognition of amylose helices. Structure 16, 1105–1115. [PubMed: 18611383]

Koropatkin NM, Cameron EA, and Martens EC (2012). How glycan metabolism shapes the human gut microbiota. Nat. Rev. Microbiol 10, 323–335. [PubMed: 22491358]

Langmead B, Trapnell C, Pop M, and Salzberg SL (2009). Ultrafast and memory-efficient alignment of short DNA sequences to the human genome. Genome Biol. 10, R25. [PubMed: 19261174]

Lavelle A, and Sokol H (2020). Gut microbiota-derived metabolites as key actors in inflammatory bowel disease. Nat. Rev. Gastroenterol. Hepatol 17, 223–237. [PubMed: 32076145]

Leshem A, Liwinski T, and Elinav E (2020). Immune-Microbiota Interplay and Colonization Resistance in Infection. Mol. Cell 78, 597–613. [PubMed: 32208169]

Li H, and Durbin R (2009). Fast and accurate short read alignment with Burrows-Wheeler transform. Bioinformatics 25, 1754–1760. [PubMed: 19451168]

Lim B, Zimmermann M, Barry NA, and Goodman AL (2017). Engineered Regulatory Systems Modulate Gene Expression of Human Commensals in the Gut. Cell 169, 547–558.e15. [PubMed: 28431252]

Liu X, Sadhukhan S, Sun S, Wagner GR, Hirschey MD, Qi L, Lin H, and Locasale JW (2015). High-Resolution Metabolomics with Acyl-CoA Profiling Reveals Widespread Remodeling in Response to Diet. Mol. Cell. Proteomics 14, 1489–1500. [PubMed: 25795660]

Lloyd-Price J, Arze C, Ananthakrishnan AN, Schirmer M, Avila-Pacheco J, Poon TW, Andrews E, Ajami NJ, Bonham KS, Brislawn CJ, et al. ; IBDMDB Investigators (2019). Multi-omics of the gut microbial ecosystem in inflammatory bowel diseases. Nature 569, 655–662. [PubMed: 31142855]

Love MI, Huber W, and Anders S (2014). Moderated estimation of fold change and dispersion for RNA-seq data with DESeq2. Genome Biol. 15, 550. [PubMed: 25516281]

Macpherson AJ, de Agüero MG, and Ganal-Vonarburg SC (2017). How nutrition and the maternal microbiota shape the neonatal immune system. Nat. Rev. Immunol 17, 508–517. [PubMed: 28604736]

Marcobal A, Barboza M, Sonnenburg ED, Pudlo N, Martens EC, Desai P, Lebrilla CB, Weimer BC, Mills DA, German JB, and Sonnenburg JL (2011). Bacteroides in the infant gut consume milk oligosaccharides via mucus-utilization pathways. Cell Host Microbe 10, 507–514. [PubMed: 22036470]

Martin M (2011). Cutadapt removes adapter sequences from high-throughput sequencing reads. EMBnet. Journal 17, 10–12.

Mazmanian SK, Round JL, and Kasper DL (2008). A microbial symbiosis factor prevents intestinal inflammatory disease. Nature 453, 620–625. [PubMed: 18509436]

Mimee M, Tucker AC, Voigt CA, and Lu TK (2016). Programming a Human Commensal Bacterium, Bacteroides thetaiotaomicron, to Sense and Respond to Stimuli in the Murine Gut Microbiota. Cell Syst. 2, 214. [PubMed: 27135367]

Author Manuscript Author Manuscript Author Manuscript Author Manuscript

Pal D, Venkova-Canova T, Srivastava P, and Chattoraj DK (2005). Multipartite regulation of *rctB*, the replication initiator gene of *Vibrio cholerae* chromosome II. J. Bacteriol 187, 7167–7175. [PubMed: 16237000]

Pamer EG (2016). Resurrecting the intestinal microbiota to combat antibiotic-resistant pathogens. Science 352, 535–538. [PubMed: 27126035]

Pantosti A, Tzianabos AO, Onderdonk AB, and Kasper DL (1991). Immunochemical characterization of two surface polysaccharides of Bacteroides fragilis. Infect. Immun 59, 2075–2082. [PubMed: 2037368]

Pasolli E, Asnicar F, Manara S, Zolfo M, Karcher N, Armanini F, Beghini F, Manghi P, Tett A, Ghensi P, et al. (2019). Extensive Unexplored Human Microbiome Diversity Revealed by Over 150,000 Genomes from Metagenomes Spanning Age, Geography, and Lifestyle. Cell 176, 649–662.e20. [PubMed: 30661755]

Patnode ML, Beller ZW, Han ND, Cheng J, Peters SL, Terrapon N, Henrissat B, Le Gall S, Saulnier L, Hayashi DK, et al. (2019). Interspecies Competition Impacts Targeted Manipulation of Human Gut Bacteria by Fiber-Derived Glycans. Cell 179, 59–73.e13. [PubMed: 31539500]

Plichta DR, Graham DB, Subramanian S, and Xavier RJ (2019). Therapeutic Opportunities in Inflammatory Bowel Disease: Mechanistic Dissection of Host-Microbiome Relationships. Cell 178, 1041–1056. [PubMed: 31442399]

Porter NT, and Martens EC (2017). The Critical Roles of Polysaccharides in Gut Microbial Ecology and Physiology. Annu. Rev. Microbiol 71, 349–369. [PubMed: 28657886]

Rakoff-Nahoum S, Coyne MJ, and Comstock LE (2014). An ecological network of polysaccharide utilization among human intestinal symbionts. Curr. Biol 24, 40–49. [PubMed: 24332541]

Rognes T, Flouri T, Nichols B, Quince C, and Mahé F (2016). VSEARCH: a versatile open source tool for metagenomics. PeerJ 4, e2584. [PubMed: 27781170]

Rooks MG, and Garrett WS (2016). Gut microbiota, metabolites and host immunity. Nat. Rev. Immunol 16, 341–352. [PubMed: 27231050]

Sato M, Yoshida Y, Nagano K, Hasegawa Y, Takebe J, and Yoshimura F (2016). Three CoA Transferases Involved in the Production of Short Chain Fatty Acids in Porphyromonas gingivalis. Front. Microbiol 07.

Sberro H, Fremin BJ, Zlitni S, Edfors F, Greenfield N, Snyder MP, Pavlopoulos GA, Kyrpides NC, and Bhatt AS (2019). Large-Scale Analyses of Human Microbiomes Reveal Thousands of Small, Novel Genes. Cell 178, 1245–1259.e14. [PubMed: 31402174]

Schmidt TSB, Raes J, and Bork P (2018). The Human Gut Microbiome: From Association to Modulation. Cell 172, 1198–1215. [PubMed: 29522742]

Schwalm ND 3rd, Townsend GE 2nd, and Groisman EA (2017). Prioritization of polysaccharide utilization and control of regulator activation in Bacteroides thetaiotaomicron. Mol. Microbiol 104, 32–45. [PubMed: 28009067]

Sherwin E, Bordenstein SR, Quinn JL, Dinan TG, and Cryan JF (2019). Microbiota and the social brain. Science 366, eaar2016. [PubMed: 31672864]

Shishkin AA, Giannoukos G, Kucukural A, Ciulla D, Busby M, Surka C, Chen J, Bhattacharyya RP, Rudy RF, Patel MM, et al. (2015). Simultaneous generation of many RNA-seq libraries in a single reaction. Nat. Methods 12, 323–325. [PubMed: 25730492]

Simon R, Priefer U, and Pühler A (1983). A Broad Host Range Mobilization System for In Vivo Genetic Engineering: Transposon Mutagenesis in Gram Negative Bacteria. Nature Biotechnology 1, 784–791.

Smith CJ, Rogers MB, and McKee ML (1992). Heterologous gene expression in Bacteroides fragilis. Plasmid 27, 141–154. [PubMed: 1615064]

Smith PM, Howitt MR, Panikov N, Michaud M, Gallini CA, Bohlooly-Y M, Glickman JN, and Garrett WS (2013). The microbial metabolites, short-chain fatty acids, regulate colonic Treg cell homeostasis. Science 341, 569–573. [PubMed: 23828891]

Sonnenburg JL, and Bäckhed F (2016). Diet-microbiota interactions as moderators of human metabolism. Nature 535, 56–64. [PubMed: 27383980]

Author Manuscript Author Manuscript Author Manuscript Author Manuscript

Sonnenburg ED, Zheng H, Joglekar P, Higginbottom SK, Firbank SJ, Bolam DN, and Sonnenburg JL (2010). Specificity of polysaccharide use in intestinal bacteroides species determines diet-induced microbiota alterations. Cell 141, 1241–1252. [PubMed: 20603004]

Sorbara MT, Dubin K, Littmann ER, Moody TU, Fontana E, Seok R, Leiner IM, Taur Y, Peled JU, van den Brink MRM, et al. (2019). Inhibiting antibiotic-resistant Enterobacteriaceae by microbiota-mediated intracellular acidification. J. Exp. Med 216, 84–98. [PubMed: 30563917]

Stokes JM, Lopatkin AJ, Lobritz MA, and Collins JJ (2019). Bacterial Metabolism and Antibiotic Efficacy. Cell Metab. 30, 251–259. [PubMed: 31279676]

Suzek BE, Huang H, McGarvey P, Mazumder R, and Wu CH (2007). UniRef: comprehensive and non-redundant UniProt reference clusters. Bioinformatics 23, 1282–1288. [PubMed: 17379688]

Suzek BE, Wang Y, Huang H, McGarvey PB, and Wu CH; UniProt Consortium (2015). UniRef clusters: a comprehensive and scalable alternative for improving sequence similarity searches. Bioinformatics 31, 926–932. [PubMed: 25398609]

West-Eberhard MJ (2019). Modularity as a universal emergent property of biological traits. J. Exp. Zoolog. B Mol. Dev. Evol 332, 356–364.

Wexler AG, and Goodman AL (2017). An insider's perspective: Bacteroides as a window into the microbiome. Nat. Microbiol 2, 17026. [PubMed: 28440278]

Woltereck R (1909). Weitere experimentelle Unter-suchungen uber Artveranderung, speziell uber das Wesen quantitativer Artunterschiede bei Daphniden. Verh Tsch Zool Ges, 110–172.

Wu M, McNulty NP, Rodionov DA, Khoroshkin MS, Griffin NW, Cheng J, Latreille P, Kerstetter RA, Terrapon N, Henrissat B, et al. (2015). Genetic determinants of in vivo fitness and diet responsiveness in multiple human gut Bacteroides. Science 350, aac5992. [PubMed: 26430127]

Zeevi D, Korem T, Godneva A, Bar N, Kurilshikov A, Lotan-Pompan M, Weinberger A, Fu J, Wijmenga C, Zhernakova A, and Segal E (2019). Structural variation in the gut microbiome associates with host health. Nature 568, 43–48. [PubMed: 30918406]

Zhu YY, Machleder EM, Chenchik A, Li R, and Siebert PD (2001). Reverse transcriptase template switching: a SMART approach for full-length cDNA library construction. Biotechniques 30, 892–897. [PubMed: 11314272]

Ziels RM, Nobu MK, and Sousa DZ (2019). Elucidating Syntrophic Butyrate-Degrading Populations in Anaerobic Digesters Using Stable-Isotope-Informed Genome-Resolved Metagenomics. mSystems 4, e00159–18. [PubMed: 31387934]

Zimmermann M, Zimmermann-Kogadeeva M, Wegmann R, and Goodman AL (2019). Mapping human microbiome drug metabolism by gut bacteria and their genes. Nature 570, 462–467. [PubMed: 31158845]

Zitvogel L, Ma Y, Raoult D, Kroemer G, and Gajewski TF (2018). The microbiome in cancer immunotherapy: Diagnostic tools and therapeutic strategies. Science 359, 1366–1370. [PubMed: 29567708]

Author Manuscript Author Manuscript Author Manuscript Author Manuscript

Highlights

- Butyrate inhibits gut microbiome *Bacteroides*
- Butyrate inhibition depends on which sugar a given *Bacteroides* strain uses
- Core genome variation in Acyl-CoA enzymes mediates butyrate defense
- Each *Bacteroides* unique fitness landscape unpredictable by interaction of ecosystem parts

Author Manuscript Author Manuscript Author Manuscript Author Manuscript

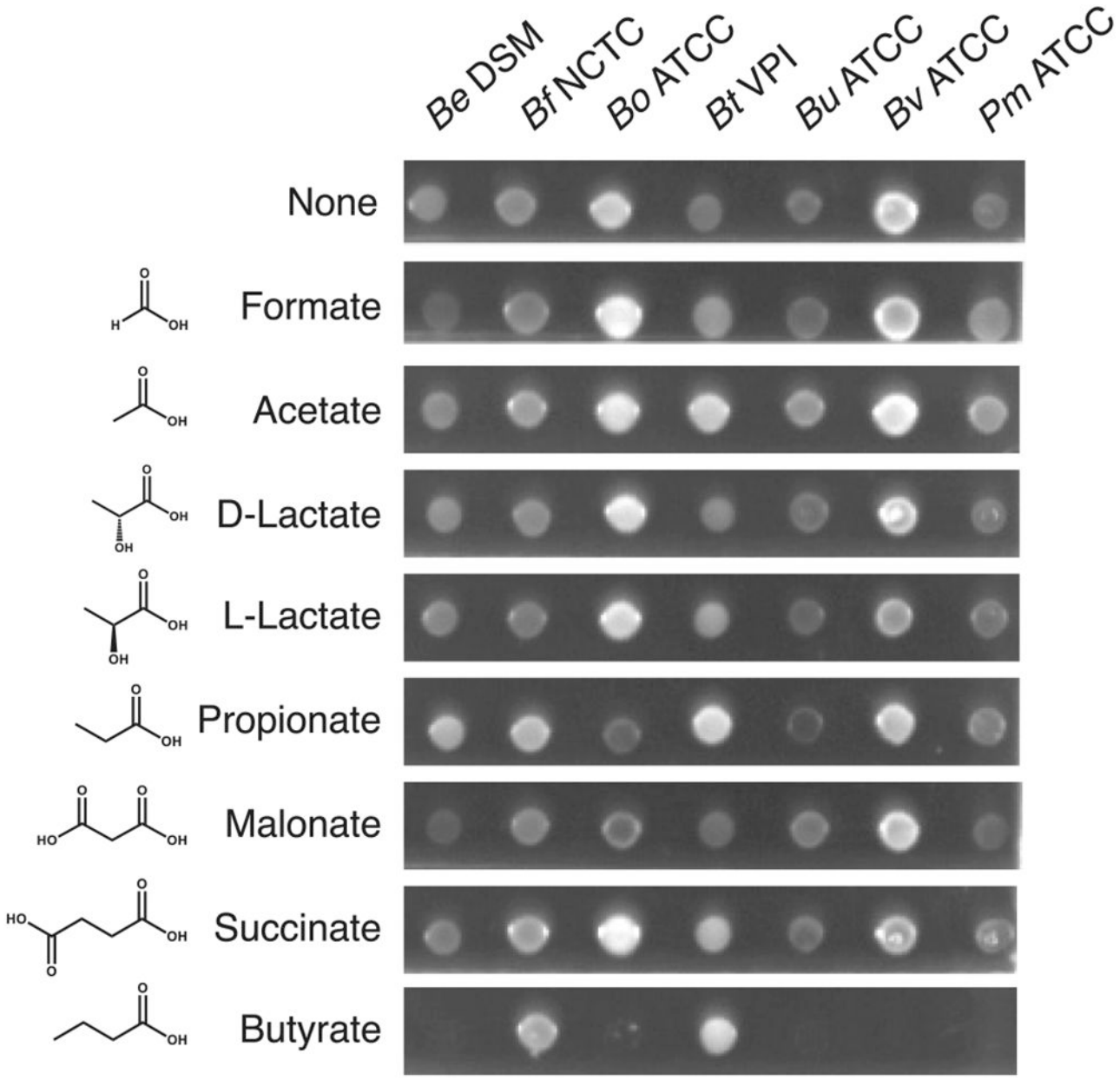

Figure 1. The effect of microbial metabolites on growth of Bacteriodales

Type strains of Bacteriodales were grown in the presence or absence of SCFAs with Glc as the carbon source. *Be* DSM: *B. eggerthii* DSM 20697, *Bf* NCTC: *B. fragilis* NCTC 9343, *Bo* ATCC: *B. ovatus* ATCC 8483, *Bt* VPI: *B. thetaiotaomicron* VPI-5482, *Bu* ATCC: *B. uniformis* ATCC 8492, *Bv* ATCC: *B. vulgatus* ATCC 8482, *Pm* ATCC: *P. merdae* ATCC 43184. Shown is a representative of three biological replicates.

Author Manuscript Author Manuscript Author Manuscript Author Manuscript

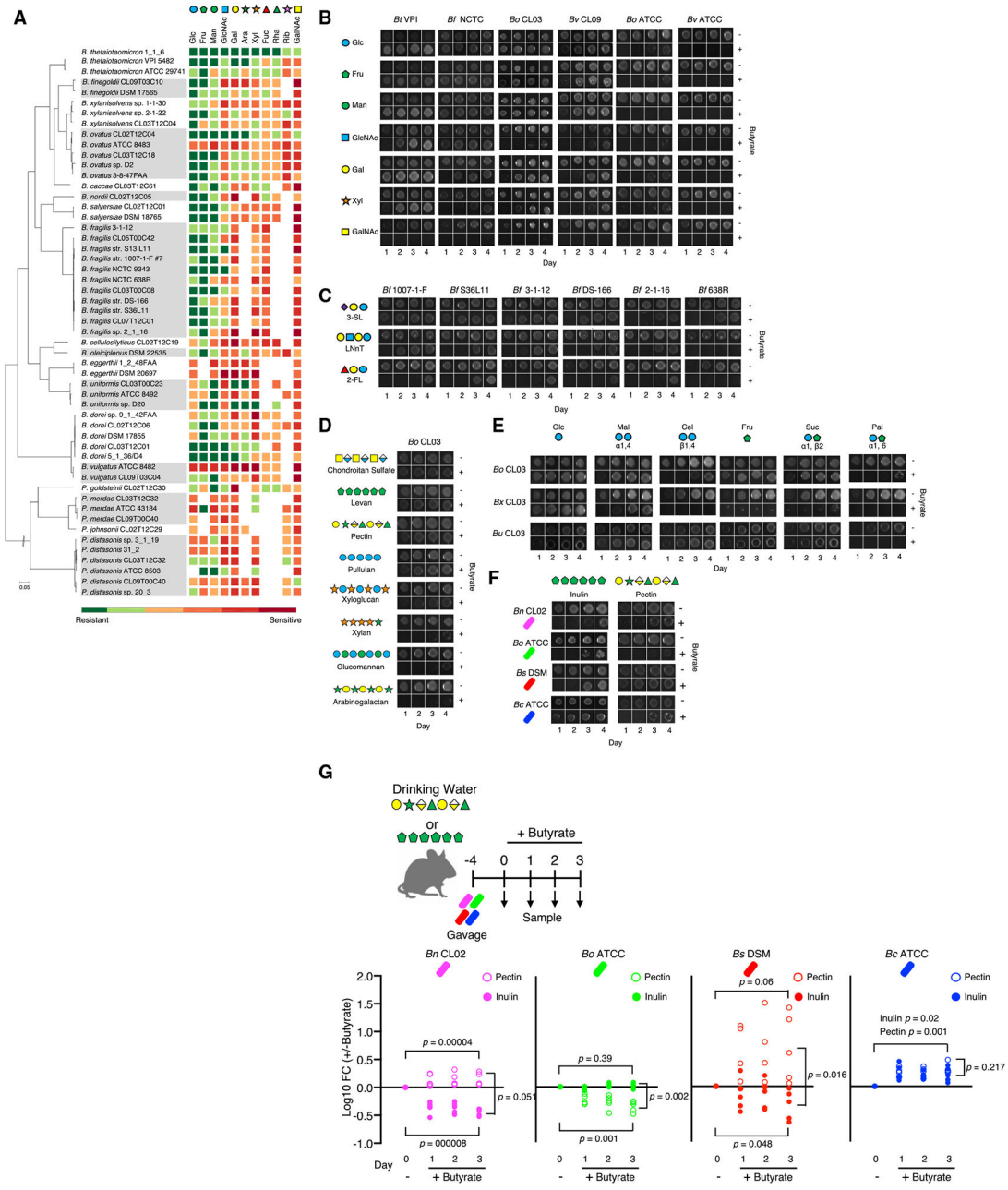

Figure 2. Strain-level fitness in the *Bacteroides* is dependent on the interactions of sugars and butyrate

(A) Heatmap of sensitivity to butyrate as a function of monosaccharide utilization (See STAR Methods for details on inhibition scoring). Row presents the phylogenic tree of the *Bacteroides* and *Parabacteroides*.

(B–E) Strains as indicated were grown in monosaccharides (B), human milk oligosaccharides (C), glycans (D), and monosaccharides and cognate homodimers disaccharides (E) with and without butyrate. See also Figures S1D and S1E.

(F) *B. nordii* CL02, *B. ovatus* ATCC, *B. salyersiae* DSM, and *B. caccae* ATCC grown in inulin or pectin −/+ butyrate.

Author Manuscript Author Manuscript Author Manuscript Author Manuscript

(G) Schematic of gnotobiotic experiments (top). Log fold change of relative abundance (post/pre butyrate in drinking water for given dietary glycan) of *Bn* CL02, *Bo* ATCC, *Bs* DSM, and *Bc* ATCC (bottom). *p* value by two-tailed Student's t test as indicated (n = 5/group). See STAR Methods for details.

Shown is a representative of two biological replicates in (A–F).

Author Manuscript Author Manuscript Author Manuscript Author Manuscript

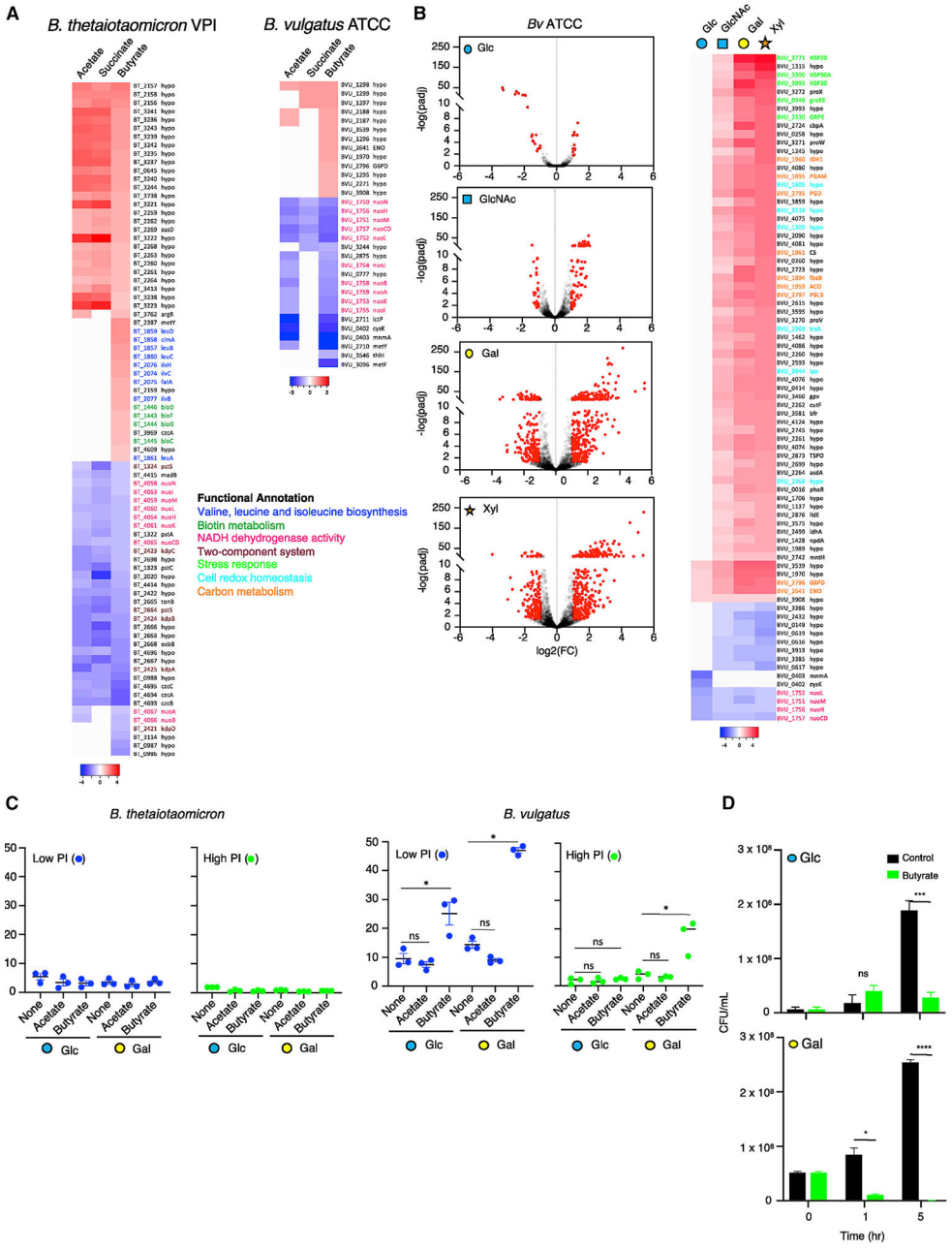

Figure 3. Butyrate induces sugar-dependent stress responses and membrane damage

(A) RNA-seq of *Bt* VPI (left) and *Bv* ATCC (right) after 1 h pulse with and without specific SCFAs in Glc. Heatmap illustrates expression of genes regulated by butyrate (|log2(fold change)|> 1, p_{adj} < 0.05) and the differential expression of these genes in acetate and/or succinate. See also Figure S2A and Table S2.

(B) RNA-seq of *Bv* ATCC after 1 h pulse −/+ butyrate in various sugars. Volcano plots showing the significance and fold change of genes in each sugar condition (right). Significantly differentially expressed genes are shown in red (|log2(fold change)|> 1, p_{adj} < 0.05). Heatmap illustrates gradient of differential expression of significant genes across sugars in response to butyrate (left). See also Table S2 and STAR Methods.

Author Manuscript Author Manuscript Author Manuscript Author Manuscript

(C) Scatterplot of flow cytometry analysis of low and high propidium iodide (PI) staining of *Bt* VPI and *Bv* ATCC with and without specific SCFAs in Glc or Gal. See also Figure S2C and STAR Methods for gating strategy.

(D) Colony forming units of *Bv* ATCC after pulse −/+ butyrate in Glc or Gal.

In (A and B), fold change and p_{adj} were calculated for two biological replicates. In (C and D), error bars represent mean ± SEM of three biological replicates. Nonsignificant $p > 0.05$, *$p < 0.05$, ***$p < 0.001$, ****$p < 0.0001$; paired two-tailed t test.

Author Manuscript Author Manuscript Author Manuscript Author Manuscript

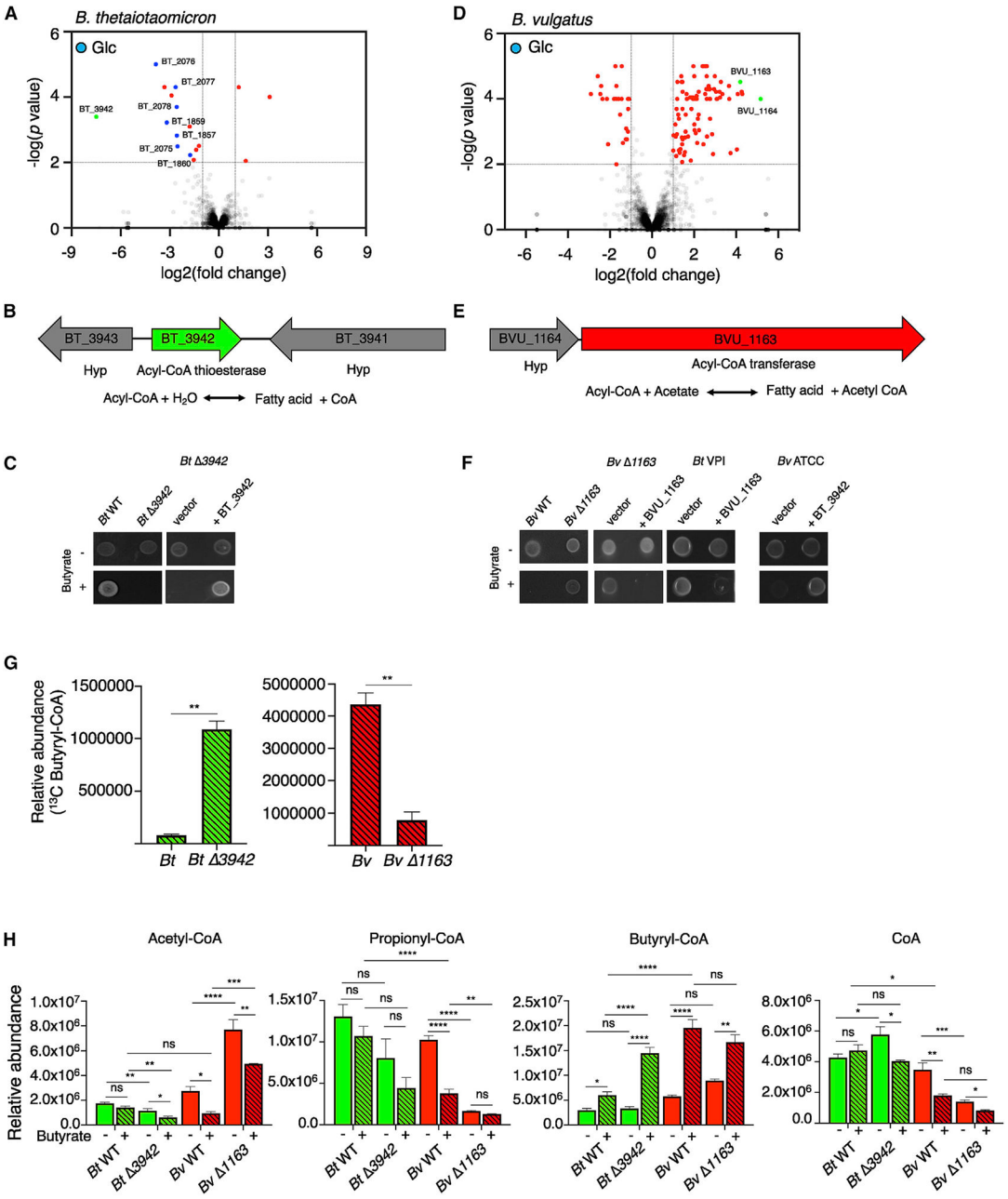

Figure 4. An Acyl-CoA metabolic defense system in the *Bacteroides*

(A) Tn-seq of *Bt* VPI grown in Glc −/+ butyrate. Specific genes are highlighted in green (BT_3942) and blue (*ilv* and *leu* operons). See also Table S3.

(B) Genomic locus of BT_3942 encoding Acyl-CoA thioesterase and predicted enzymatic reaction.

(C) *Bt* WT, *Bt* Δ3942 and the complemented strain grown in Glc −/+ butyrate.

(D) Tn-seq of *Bv* ATCC grown in Glc −/+ butyrate. Specific genes are highlighted in green (BVU_1164/ 1163 operon). See also Table S3.

(E) Genomic locus of the BVU_1164/1163 operon encoding a hypothetical protein and Acyl-CoA transferase and predicted enzymatic reaction.

Author Manuscript Author Manuscript Author Manuscript Author Manuscript

(F) *Bv* WT, *Bv* Δ1163, and the complemented strain (two left), and *Bt* WT complemented with BVU_1163 (third from left). *Bv* Δ1163 complemented with BT_3942 (right) grown in Glc −/+ butyrate.

(G) Relative abundance of ^{13}C butyryl-CoA in *Bt* WT, *Bv* WT, and their isogenic mutant strains 30 min post pulse at mid log phase in Glc with ^{13}C butyrate. See also Figure S3E.

(H) Relative abundance of Acyl-CoAs in *Bt* WT, *Bv* WT, and their isogenic strains, as indicated, in Glc with butyrate or water control. See also Figure S3G.

In (A and D), plots are the combined fold change and *p* value from two independent replicates (See STAR Methods). Shown is a representative of three biological replicates in (C and F). Error bars represent mean ± SEM of two (G) and three (H) biological replicates. Nonsignificant $p > 0.05$, *$p < 0.05$, **$p < 0.01$, ***$p < 0.001$, ****$p < 0.0001$; unpaired two-tailed t test in (G), two-way ANOVA with Tukey's multiple comparisons test in (H).

Author Manuscript Author Manuscript Author Manuscript Author Manuscript

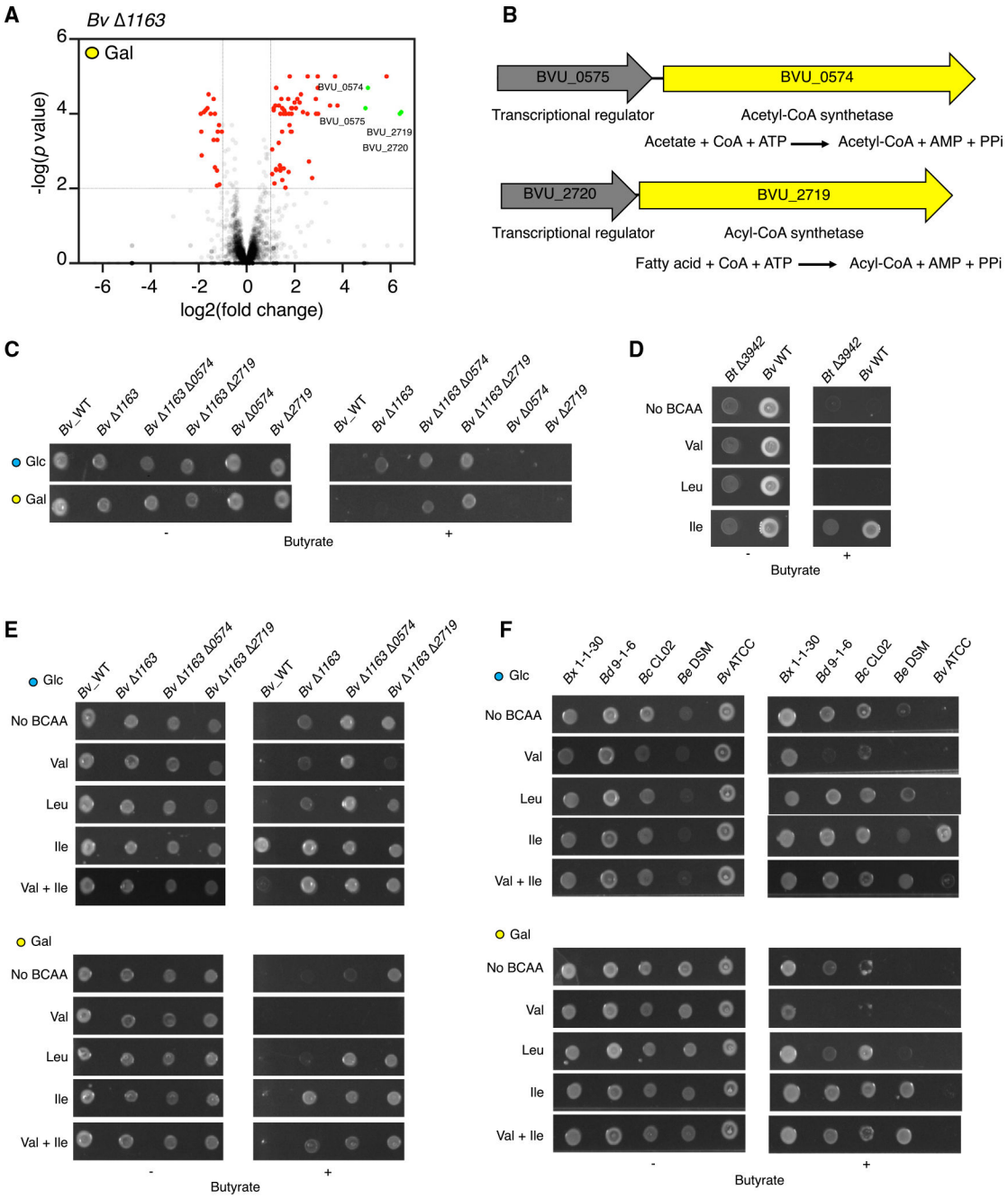

Figure 5. Synergy in Acyl-CoA metabolism interacts with BCAAs to tune sugar-dependent inhibitory effects of butyrate

(A) Tn-seq of *Bv Δ1163* grown in Gal −/+ butyrate. Two operons, BVU_0575/0574 and BVU_2720/2719, are highlighted in green. Fold change and *p* value were calculated by combining two biological replicates. See also Table S3.

(B) Genomic locus of BVU_0575/0574 encoding transcriptional regulator and Acetyl-CoA synthetase, and BVU_2720/2719 encoding transcriptional regulator and Acyl-CoA synthetase and predicted enzymatic reactions.

Author Manuscript Author Manuscript Author Manuscript Author Manuscript

(C) *Bv* WT and isogenic strains with deletions in Acyl-CoA transferase (BVU_1163) and Acyl-CoA synthetases (BVU_2719, BVU_0574) grown in Glc or Gal −/+ butyrate.
(D) *Bt* Δ3942 and *Bv* WT grown in Glc supplemented with Val, Leu, or Ile −/+ butyrate.
(E and F) *Bv* WT and isogenic strains with deletions in Acyl-CoA transferase (BVU_1163) and Acyl-CoA synthetases (BVU_2719, BVU_0574) (E) and natural human gut *Bacteroides* strains (F) grown in Glc or Gal supplemented with Val, Leu, or Ile −/+ butyrate.
Shown is a representative of three biological replicates in (C–F).

Author Manuscript Author Manuscript Author Manuscript Author Manuscript

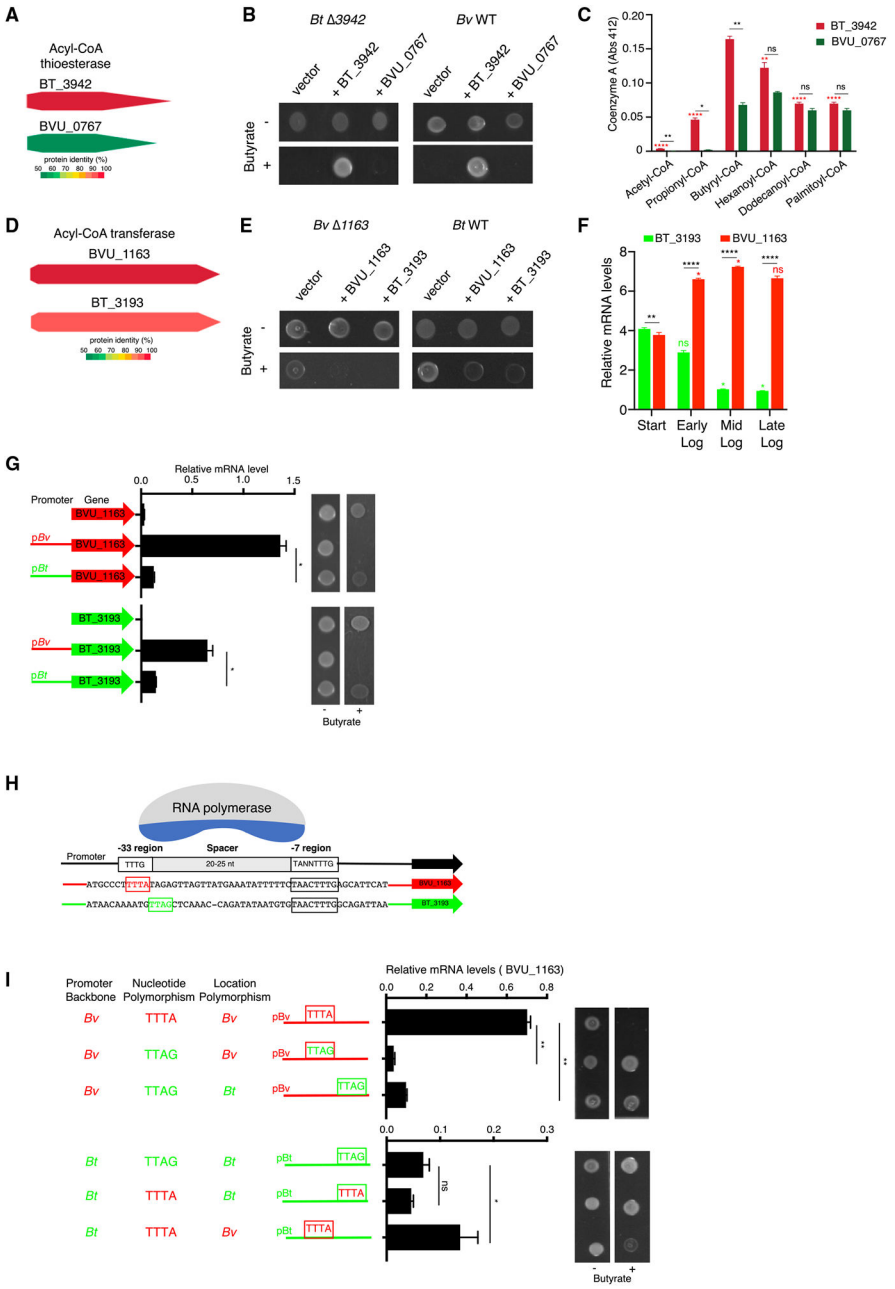

Figure 6. Species-level genetic variation in Acyl-CoA metabolic defense among the *Bacteroides*

(A) Protein identity of Acyl-CoA thioesterases, BT_3942 (*Bt* VPI), and BVU_0767 (*Bv* ATCC). See also Figures S5A and S5B.

(B) *Bt* Δ3942 and *Bv* WT complemented with BT_3942 or BVU_0767 grown in Glc −/+ butyrate.

(C) Acyl-CoA thioesterase activity of the recombinant proteins, BT_3942, and BVU_0767 with different chain lengths of acyl-CoAs as substrate. See also Figure S5C.

(D) Protein identity of Acyl-CoA transferases, BVU_1163 (*Bv* ATCC) and BT_3193 (*Bt* VPI). See also Figures S5D and S5E.

Author Manuscript Author Manuscript Author Manuscript Author Manuscript

(E) *Bv* Δ1163 and *Bt* WT complemented with BVU_1163 or BT_3193 grown in Glc −/+ butyrate.
(F) Relative mRNA expression of Acyl-CoA transferase in *Bt* VPI (BT_3193) and *Bv* ATCC (BVU_1163) grown in Glc across growth phases. See also Figure S5F.
(G) mRNA levels of Acyl-CoA transferase genes (left) and inhibitory effect of butyrate (right) in *Bv* Δ1163 strains harboring plasmids expressing BVU_1163 or BT_3193 under their native or swapped promoters.
(H) Schematic of RNA polymerase binding sites showing nucleotide polymorphisms within the promoter regions of BVU_1163 and BT_3193.
(I) Schematic of the nucleotide polymorphism constructs on p*Bv* and p*Bt* promoter backbones (left), mRNA levels of BVU_1163 (middle), and inhibitory effect of butyrate (right) in *Bv* Δ1163 strains harboring plasmids driving BVU_1163 under the promoter with each strain-specific nucleotide polymorphism.
Error bars represent mean ± SEM of two biological replicates in (C and F) and three biological replicates in (G and I). Nonsignificant $p > 0.05$, *$p < 0.05$, **$p < 0.01$, ***$p < 0.001$; unpaired two-tailed t test in (C, F, G, and I), One-Way ANOVA with Dunnett multiple comparisons test in (C, red asterisks). Shown is a representative of three biological replicates in (B, E, G, and I).

Author Manuscript Author Manuscript Author Manuscript Author Manuscript

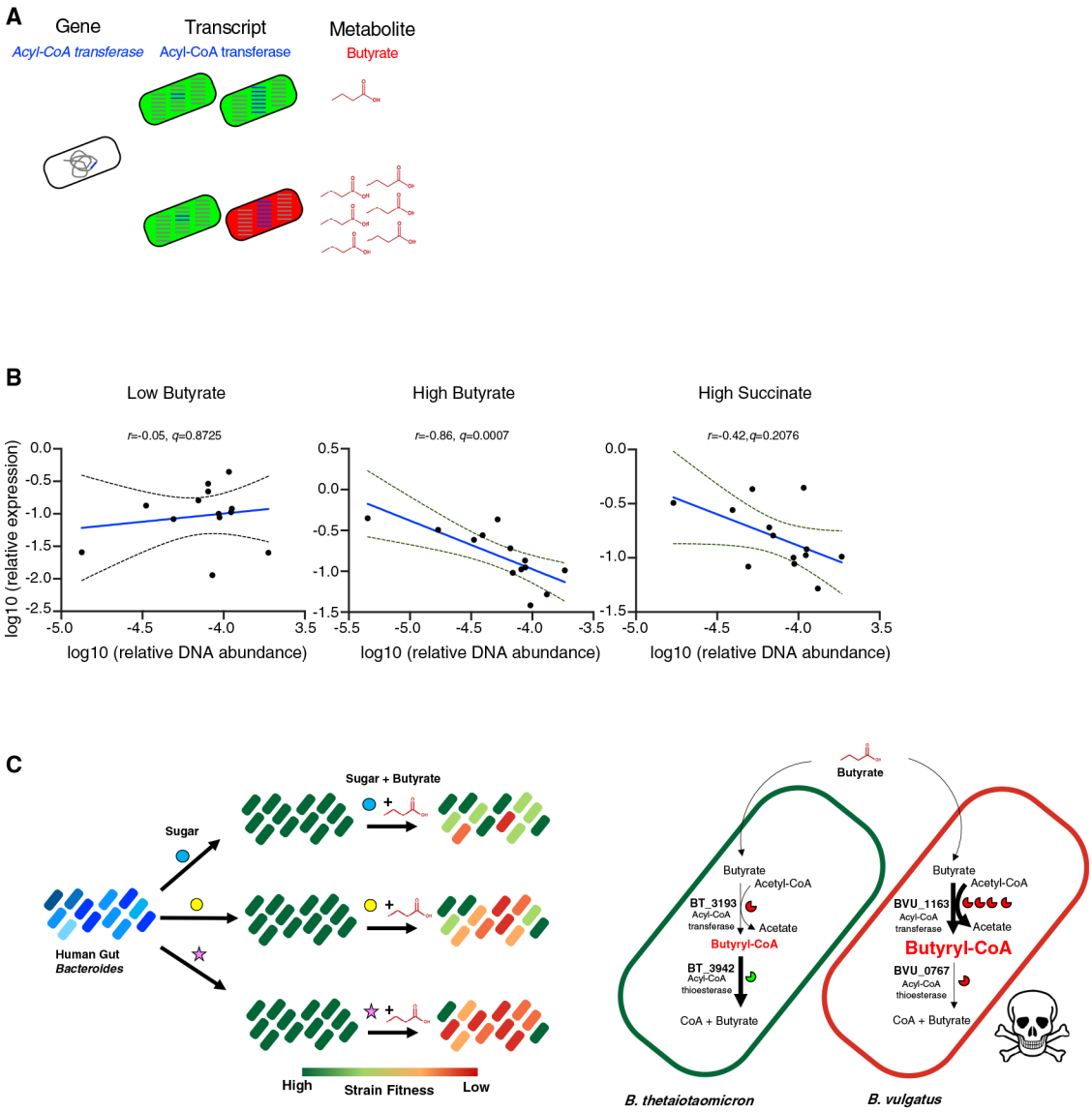

Figure 7. *Bacteroides* fitness is conditional on Acyl-CoA transferase expression and butyrate *in vivo*

(A) Schematic demonstrating *Bacteroides* fitness based on interactions of BT_3193/BVU_1163 gene function, expression, and presence of a specific metabolite butyrate. Fitness represented in green (high) and red (low).

(B) Correlation between relative DNA abundance and relative expression of the Acyl-CoA transferase BT_3193/BVU_1163 of fecal samples from 26 human subjects in low versus high levels of fecal butyrate or high succinate (Benjamini-Hochberg false discovery rate (FDR) approach with a conservative FDR q-value < 0.05). See also Figure S6A.

(C) (left) Schematic of butyrate acting as a sugar- and strain-specific fitness switch in the *Bacteroides*. For three representative sugars, for which each *Bacteroides* species/strains (indicated by shades of blue) utilize and grow (high fitness indicated in green), butyrate results in differential impact on fitness at the species and strain level. (right) Model of the genetic and molecular mechanisms mediating variation in the inhibitory effect of butyrate

among the *Bacteroides*. Butyrate enters the cell and is converted to butyryl-CoA through the activity of an Acyl-CoA transferase. An Acyl-CoA thioesterase then hydrolyzes butyryl-CoA decreasing cellular accumulation of this candidate toxic product. In the sensitive *Bv*, BVU_1163 (Acyl-CoA transferase) is highly expressed (4 enzyme symbols) leading to greater production of butyryl-CoA, and the poorly conserved Acyl-CoA thioesterase homolog in *Bv* (BVU_0767) results in butyryl-CoA accumulation.

Author Manuscript Author Manuscript Author Manuscript Author Manuscript

Author Manuscript Author Manuscript Author Manuscript Author Manuscript

KEY RESOURCES TABLE

REAGENT or RESOURCE	SOURCE	IDENTIFIER
Bacterial strains		
Bacteroides thetaiotaomicron 1_1_6	BEI	HM-23
Bacteroides thetaiotaomicron VPI-5482	ATCC	ATCC 29148
Bacteroides thetaiotaomicron ATCC 29741	ATCC	ATCC 29741
Bacteroides finegoldii CL09T03C10	BEI	HM-727
Bacteroides finegoldii DSM 17564	DSMZ	DSM 17564
Bacteroides xylanisolvens sp. 1_1_30	BEI	HM-22
Bacteroides xylanisolvens sp. 2_1_22	BEI	HM-18
Bacteroides xylanisolvens CL03T12C04	BEI	HM-722
Bacteroides ovatus CL02T12C04	BEI	HM-723
Bacteroides ovatus ATCC 8483	ATCC	ATCC 8483
Bacteroides ovatus CL03T12C18	BEI	HM-724
Bacteroides ovatus sp. D2	BEI	HM-28
Bacteroides ovatus 3_8_47FAA	BEI	HM-222
Bacteroides caccae ATCC 43185	ATCC	ATCC 43185
Bacteroides caccae CL03T12C61	BEI	HM-728
Bacteroides nordii CL02T12C05	BEI	HM-721
Bacteroides salyersiae CL02T12C01	BEI	HM-725
Bacteroides salyersiae DSM 18765	DSMZ	DSM 18765
Bacteroides fragilis 3_1_12	BEI	HM-20
Bacteroides fragilis CL05T00C42	BEI	HM-711
Bacteroides fragilis str. S13 L11	Lab of Laurie E. Comstock	(Coyne et al., 2016)
Bacteroides fragilis str. 1007-1-F #7	Lab of Laurie E. Comstock	(Coyne et al., 2016)
Bacteroides fragilis NCTC 9343	ATCC	ATCC25825
Bacteroides fragilis NCTC 638R	Lab of Laurie E. Comstock	(Coyne et al., 2016)
Bacteroides fragilis CL03T00C08	BEI	HM-713
Bacteroides fragilis str. DS-166	Lab of Laurie E. Comstock	(Coyne et al., 2016)
Bacteroides fragilis str. S36L11	Lab of Laurie E. Comstock	(Coyne et al., 2016)
Bacteroides fragilis CL07T00C01	BEI	HM-709
Bacteroides fragilis sp. 2_1_16	BEI	HM-58
Bacteroides cellulosilyticus CL02T12C19	BEI	HM-726
Bacteroides oleiciplenus DSM 22535	DSMZ	DSM 22535
Bacteroides eggerthii 1_2_48FAA	BEI	HM-201
Bacteroides eggerthii DSM 20697	DSMZ	DSM 20697
Bacteroides uniformis CL03T00C23	BEI	HM-715
Bacteroides uniformis ATCC 8492	ATCC	ATCC 8492
Bacteroides uniformis sp. D20	BEI	HM-189
Bacteroides dorei sp. 9_1_42FAA	BEI	HM-27
Bacteroides dorei CL02T00C15	BEI	HM-717
Bacteroides dorei DSM 17855	DSMZ	DSM 17855

Author Manuscript Author Manuscript Author Manuscript Author Manuscript

REAGENT or RESOURCE	SOURCE	IDENTIFIER
Bacteroides dorei CL03T12C01	BEI	HM-718
Bacteroides dorei 5_1_36/D4	BEI	HM-29
Bacteroides vulgatus ATCC 8482	ATCC	ATCC 8482
Bacteroides vulgatus CL09T03C04	BEI	HM-720
Parabacteroides goldsteinii CL02T12C30	BEI	HM-732
Parabacteroides merdae CL03T12C32	BEI	HM-730
Parabacteroides merdae ATCC 43184	ATCC	ATCC 43184
Parabacteroides merdae CL09T00C40	BEI	HM-729
Parabacteroides johnsonii CL02T12C29	BEI	HM-731
Parabacteroides distasonis sp. 3_1_19	BEI	HM-19
Parabacteroides distasonis 31_2	BEI	HM-169
Parabacteroides distasonis CL03T12C09	BEI	HM-733
Parabacteroides distasonis ATCC 8503	ATCC	ATCC 8503
Parabacteroides distasonis CL09T03C24	BEI	HM-734
Parabacteroides distasonis sp. 20_3	BEI	HM-166
Bt VIP Δ*3942*	This study	N/A
Bv ATCC Δ*1163*	This study	N/A
Bv ATCC Δ*1163* Δ*0574*	This study	N/A
Bv ATCC Δ*1163* Δ*2719*	This study	N/A
Bv ATCC Δ*0574*	This study	N/A
Bv ATCC Δ*2719*	This study	N/A
Bv ATCC Δ*1163 att1*:: pNBU2-*erm*_TetR-p1T_DP-GH023_BVU_1163	This study	N/A
Bv ATCC Δ*1163* Δ*0574 att1*:: pNBU2-*erm*_TetR-p1T_DP-GH023_BVU_1163	This study	N/A
Bv CL09 Δ*1163*	This study	N/A
Bv CL09 Δ*2719*	This study	N/A
Bv CL09 Δ*1163* Δ*2719*	This study	N/A
Escherichia coli DH5a λ pir	(Pal et al., 2005)	N/A
Escherichia coli S17-1 λ pir	(Simon et al., 1983)	N/A
Escherichia coli BL21 (DE3)	Novagen	C600003
Chemicals and recombinant proteins		
Brain Heart Infusion	BD Bioscience	Cat# 237500
Sodium formate	Sigma-Aldrich	Cat# 107603
Sodium acetate	Sigma-Aldrich	Cat# S2889
Sodium D-lactate	Sigma-Aldrich	Cat# 71716
Sodium L-lactate	Sigma-Aldrich	Cat# 71718
Sodium propionate	Sigma-Aldrich	Cat# P1880
Sodium malonate dibasic	Sigma-Aldrich	Cat# 63409
Sodium succinate dibasic hexahydrate	Sigma-Aldrich	Cat# S9637
Sodium butyrate	Sigma-Aldrich	Cat# 303410
Sodium butyrate (^{13}C4)	Cambridge *Isotope Laboratories*	Cat# CLM-10426-0.1
Glucose	Sigma-Aldrich	Cat# G7021
Fructose	Sigma-Aldrich	Cat# F3510

Author Manuscript Author Manuscript Author Manuscript Author Manuscript

REAGENT or RESOURCE	SOURCE	IDENTIFIER
Mannose	Sigma-Aldrich	Cat# M6020
N-Acetylglucosamine	Sigma-Aldrich	Cat# A3286
Galactose	Sigma-Aldrich	Cat# G5388
Arabinose	Sigma-Aldrich	Cat# A3131
Xylose	Sigma-Aldrich	Cat# X3877
Fucose	Sigma-Aldrich	Cat# F2252
Rhamnose	Sigma-Aldrich	Cat# R3875
Ribose	Sigma-Aldrich	Cat# D5251
N-Acetylgalactosamine	Sigma-Aldrich	Cat# A2795
3-Sialyllactose (3-SL)	GLYCOM	Cat# GlyCare™ 3SL
Lacto-N-neotetraose (LNnT)	GLYCOM	Cat# GlyCare™ LNnT
2-fucosyllactose (2-FL)	GLYCOM	Cat# GlyCare™ 2FL
Pullulan	Sigma-Aldrich	Cat# P4516
Levan	Sigma-Aldrich	Cat# L8647
Xylan	Sigma-Aldrich	Cat# X4252
Xyloglucan (Tamarind)	Megazyme	Cat# P-XYGLN
Arabinan (Sugar beet)	Megazyme	Cat# P-ARAB
Arabinogalactan (Larch Wood)	Megazyme	Cat# P-ARGAL
Chondroitan sulfate	Sigma-Aldrich	Cat# R7500
Inulin	Beneo	Cat# Orafti P95
Pectin	Sigma-Aldrich	Cat# P9135
Mannan	Sigma-Aldrich	Cat# M7504
Glucomannan	Megazyme	Cat# p-GLCML
Isoleucine	Sigma-Aldrich	Cat# I2752
Leucine	Sigma-Aldrich	Cat# L8000
Valine	Sigma-Aldrich	Cat# V0500
Maltose	Sigma-Aldrich	Cat# M5895
Sucrose	Sigma-Aldrich	Cat# S7903
Palatinose	Sigma-Aldrich	Cat# P2007
Isopropyl β-D-1-thiogalactopyranoside	Sigma-Aldrich	Cat# I6758
4-chloro-phenylalanine	Sigma-Aldrich	Cat# C6506
5,5′-dithiobis (2-nitrobenzoic acid)	Sigma-Aldrich	Cat# D8130
Acetyl coenzyme A	Sigma-Aldrich	Cat# A2181
Propionyl coenzyme A	Sigma-Aldrich	Cat# P5397
Butyryl coenzyme A	Sigma-Aldrich	Cat# B1508
Succinyl coenzyme A	Sigma-Aldrich	Cat# S1129
Hexanoyl coenzyme A	Sigma-Aldrich	Cat# H2012
Decanoyl coenzyme A	Sigma-Aldrich	Cat# D5269
Palmitoyl coenzyme A	Sigma-Aldrich	Cat# P9716
BCECF, AM (2',7'-Bis-(2 Carboxyethyl)-5-(and-6)-Carboxyfluorescein, Acetoxymethyl Ester)	Thermo Fisher Scientific	Cat# B1151
Nigericin	Sigma-Aldrich	Cat# N7143

Author Manuscript Author Manuscript Author Manuscript Author Manuscript

REAGENT or RESOURCE	SOURCE	IDENTIFIER
Valinomycin	Sigma-Aldrich	Cat# V0627
Propidium Iodide	Thermo Fisher Scientific	Cat# P3566
BT_3942-His tag	This study	N/A
BVU_0767-His tag	This study	N/A
Antibodies		
Anti-HA	Santa Cruz	Cat# sc-7392
Anti-*E. coli* RpoA	BioLegend	Cat# 663104
Critical commercial assays		
SuperScript VI Reverse Transcriptase	Thermo Fisher Scientific	Cat# 18090200
Fast SYBR Green Master Mix	Applied Biosystem/ Thermo Fisher Scientific	Cat# 4385617
Ribo-Zero rRNA Removal Kit	Epicenter	Cat# RZH1046
PureLink Genomic DNA mini kit	Thermo Fisher Scientific	Cat# K182002
GeneArt Seamless Cloning and Assembly Enzyme Kit	Thermo Fisher Scientific	Cat# A14606
Zymo DNA Clean and Concentrator Kits	Zymo Research	Cat# D4013
ZymoBIOMICS DNA Miniprep Kit	Zymo Research	Cat# D4301
NEBNext Ultra DNA Library Prep Kit	New England Biolabs	Cat# E7370
AMPure XP beads	Beckman Coulter Inc.	Cat# A63880
NEBNext Library Quant Kit for Illumina	New England Biolabs	Cat# E7630
Platinum SuperFi PCR Master Mix	Thermo Fisher Scientific	Cat# 12358250
Direct-zol RNA Miniprep Plus Kit	Zymo Research	Cat# R2072
HisPur Ni-NTA Resin	Thermo Fisher Scientific	Cat# 88221
Halt Protease Inhibitor Cocktail	Thermo Fisher Scientific	Cat# PI87786
NuPAGE 4 to 12%, Bis-Tris Mini Protein Gel	Thermo Fisher Scientific	Cat# NP0322BOX
Deposited data		
The raw RNA_Seq and Tn_Seq data	NCBI BioProject ID	PRJNA640947
Tn-Seq_*B. thetaiotaomicron* VPI-5482/Glucose	NCBI BioProject ID	PRJNA640947
Tn-Seq_*B. vulgatus* ATCC 8482/Glucose	NCBI BioProject ID	PRJNA640947
Tn-Seq_*Bv* ΔBVU_1163/Galactose	NCBI BioProject ID	PRJNA640947
sTn-Seq_*B. vulgatus* CL09/Galactose	NCBI BioProject ID	PRJNA640947
RNA-Seq_ *B. thetaiotaomicron* VPI-5482/Glucose/Acetate	NCBI BioProject ID	PRJNA640947
RNA-Seq_ *B. thetaiotaomicron* VPI-5482/Glucose/Succinate	NCBI BioProject ID	PRJNA640947
RNA-Seq_ *B. thetaiotaomicron* VPI-5482/Glucose/Butyrate	NCBI BioProject ID	PRJNA640947
RNA-Seq_ *B. thetaiotaomicron* VPI-5482/Galactose	NCBI BioProject ID	PRJNA640947
RNA-Seq_ *B. vulgatus* ATCC 8482/Glucose/Acetate	NCBI BioProject ID	PRJNA640947
RNA-Seq_ *B. vulgatus* ATCC 8482/Glucose/Succinate	NCBI BioProject ID	PRJNA640947
RNA-Seq_ *B. vulgatus* ATCC 8482/Glucose/Butyrate	NCBI BioProject ID	PRJNA640947
RNA-Seq_ *B. vulgatus* ATCC 8482/GlNAC/Butyrate	NCBI BioProject ID	PRJNA640947
RNA-Seq_ *B. vulgatus* ATCC 8482/Galactose/Butyrate	NCBI BioProject ID	PRJNA640947
RNA-Seq_ *B. vulgatus* ATCC 8482/Xylose/Butyrate	NCBI BioProject ID	PRJNA640947
RNA-Seq_ *B. vulgatus* CL09 /Glucose/Butyrate	NCBI BioProject ID	PRJNA640947
Oligonucleotides		

Author Manuscript Author Manuscript Author Manuscript Author Manuscript

REAGENT or RESOURCE	SOURCE	IDENTIFIER
Primers used in this study	This study	Table S1
Recombinant DNA		
pRK231	(Smith et al., 1992)	N/A
pKNOCK-*bla-erm*Gb	(Koropatkin et al., 2008)	N/A
pKNOCK-*bla-erm*Gb_*phe*S*	This study	N/A
pSAM_BcellWH2	(Wu et al., 2015)	N/A
pFD340	(Smith et al., 1992)	N/A
pNBU2-*bla-erm*Gb	(Koropatkin et al., 2008)	N/A
pWH2-Term6	This study	N/A
pBT_3942	This study	N/A
pBVU_0767	This study	N/A
p*Bv*_1163	This study	N/A
p*Bv*_1163-HA	This study	N/A
p*Bt*_1163	This study	N/A
p*Bv*_3193	This study	N/A
p*Bt*_3193	This study	N/A
p*Bt*_3193-HA	This study	N/A
pN_1163	This study	N/A
pN_3193	This study	N/A
p*Bv*_TTAG-1163	This study	N/A
p*Bv*_TTAG_down-1163	This study	N/A
p*Bt*_TTTA-1163	This study	N/A
p*Bt*_TTTA_up-1163	This study	N/A
pNBU2-erm_TetR-p1T_DP-GH023	(Lim et al., 2017)	Addgene Cat #90324
pTetR_p1T_ BVU_1163	This study	N/A
pET-28a	Novagen	Cat# 69864-3
pET-28a_BT_3942-His	This study	N/A
pET-28a_BVU_0767-His	This study	N/A
Software and algorithms		
Prism9	GraphPad	https://www.graphpad.com/scientific-software/prism/
MEGA		https://www.megasoftware.net/
MATLAB/ R2017b	MathWorks	https://www.mathworks.com
Heatmapper	(Babicki et al., 2016)	http://www.heatmapper.ca
DAVID 6.8	(Huang et al., 2009)	https://david.ncifcrf.gov/
Other		
Anaerobic Chamber	Coy manufacturing	Vinyl Anaerobic Chamber

REAGENT or RESOURCE	SOURCE	IDENTIFIER
Microplate plate absorbance reader	BioTek Instruments	Synergy HTX multi-mode reader
QuantStudio Real-time PCR system	Applied Systems	3
Focused-ultrasonicators	Covaris	M220

Author Manuscript
Author Manuscript
Author Manuscript
Author Manuscript